Implementation of the urban parameterization scheme to the Delhi model with an improved urban morphology

T. J. Anurose[1] | A. Jayakumar[1] | Kshama Gupta[2] | Saji Mohandas[1] | Margaret A. Hendry[3] | Daniel K. E. Smith[4] | Timmy Francis[1,8] | Shweta Bhati[5,6] | Avinash N.Parde[6] | Manju Mohan[5] | A.K. Mitra[1] | Prasun Kumar Gupta[2] | Prakash Chauhan[2] | R Jenamani[7] | Sachin Ghude[6]

[1]National Centre for Medium Range Weather Forecasting, Ministry of Earth Sciences, Noida, India

[2]Indian Institute of Remote Sensing ISRO, India

[3]Met Office, Exeter, UK

[4]School of Environmental Sciences, University of East Anglia, Norwich, UK

[5]Centre for Atmospheric Sciences, Indian Institute of Technology Delhi, India

[6]Indian Institute of Tropical Meteorology, Ministry of Earth Sciences, India

[7]India Meteorological Department, New Delhi, India

[8]School of Earth and Environment, University of Leeds, UK

Correspondence
National Centre for Medium Range Weather Forecasting, Ministry of Earth Sciences, Noida - 201309, Uttar Pradesh, India
Email: anurose.tj@gov.in

Present address
National Centre for Medium Range Weather Forecasting, Ministry of Earth Sciences, Noida - 201309, Uttar Pradesh, India

The current study highlights the importance of a detailed representation of urban processes in a numerical weather prediction model and emphasizes the need for accurate urban morphology data for improving the near-surface weather prediction over Delhi, a tropical Indian city. The Met Office Reading Urban Surface Exchange Scheme (MORUSES), a two-tile urban energy budget parameterization scheme, is introduced in a high resolution (330 m) model of Delhi. A new empirical relationship is established for the MORUSES scheme from the local urban morphology of Delhi. The performance is evaluated using both the newly developed empirical relationships (MORUSES-IND) and the existing empirical relationships for the MORUSES scheme (MORUSES-LON) against the default one-tile configuration (BEST-1t) for clear and foggy events and validations are performed against ground observations. MORUSES-IND exhibits a significant improvement in the diurnal evolution of the wind speed in terms of amplitude and phase, compared to the other two configurations. The screen temperature (T_{screen}) sim-

Funding information

ulations using MORUSES-IND reduce the warm bias, especially during the evening and night hours. The root-mean-square error of T_{screen} is reduced up to 29 % using MORUSES-IND for both synoptic conditions. The diurnal cycle of surface energy fluxes is reproduced well using MORUSES-IND. The net longwave fluxes are underestimated in the model and biases are more significant during the foggy events partly due to the misrepresentation of fog. An urban cool island (UCI) effect is observed in the early morning hours during the clear sky conditions but it is not evident on foggy days. Compared to BEST-1t, MORUSES-IND represents the impact of urbanization more realistically which is reflected in the reduction of urban heat island and UCI in both synoptic conditions. Future works would improve the coupling between the urban surface energy budget and anthropogenic aerosols by introducing the MORUSES-IND in a chemistry aerosol framework model.

KEYWORDS

Urban parameterization, surface energy balance, MORUSES, Urban heat island, Delhi model

1 | INTRODUCTION

The majority of the world's population lives in cities and the urban population is expected to be around 66% by 2050. It is predicted that the developing countries will contribute nearly 60% of the population to the urban areas in the coming decades (United Nations, 2018). Hence, understanding the urban energy balance and exchanges in these regions is key to planning any climate change mitigation strategies. As the urbanization increases, these cities become increasingly vulnerable to weather extremes such as heat stress, drought and floods, attributed mostly to the modifications in surface-atmosphere energy exchanges and wind stress (Roth et al., 2017; Sati and Mohan, 2021). The complex surface morphology in the urban locations such as the built-up structures and materials used, reduced vegetation cover and enhanced anthropogenic emissions, modify the individual components of the energy balance. The urban structures induce multiple reflections of the incoming solar radiation, increase the trapping of the shortwave radiation and reduce the surface albedo (Oke, 1987). The high specific heat capacity of the concrete buildings leads to enhanced absorption of the shortwave radiation during daytime, which then radiates the heat to the ambient air, till late-night/early-morning hours, creating the distinct urban heat island (UHI) effect (Grimmond and Oke, 1999).

Also, urbanization plays an important role in the fog and smog events(Yan et al., 2020). Delhi, a fast growing city in India, witnesses frequent fog and smog events during winter with fog occurrences reported for 60% of the winter days, of which the dense fog cases account for nearly 16% (Ghude et al., 2017). The frequency of fog events have been increasing in Delhi and norther India in general (Jenamani, 2007; Mohan and Payra, 2009; Jenamani, 2012; Syed et al., 2012; Ghude et al., 2017). Gautam and Singh (2018) demonstrated a strong link between urban areas and observed holes in the fog layers. These holes in the widespread fog appears to be linked with the UHI effect - the increased surface heating is known to cause fog

dissipation (Duynkerke, 1991; Wærsted et al., 2019). The simulations of fog in rural areas have been shown to be sensitive to the parameterization of the land surface and soil properties (Steeneveld et al., 2015; Steeneveld and de Bode, 2018; Smith et al., 2021). Furthermore, the surface heat fluxes are important driving factors for the fog dissipation (Wærsted et al., 2019). High resolution modeling using enhanced orographic features together with detailed surface representation have shown improvements in the simulation of fog occurrences over Delhi (Jayakumar et al., 2018, 2019)

Hence, a realistic representation of the urban surface morphology effects on the heat, moisture, and momentum fluxes as well as the partitioning of the sensible and latent heat fluxes, are critical to improving the skill of high-resolution urban weather forecasting models. Urban land surface models (ULSMs) are generally embedded within the atmospheric models for improved representation of near-surface temperature, humidity, precipitation, wind speed, radiation and energy fluxes at the urban scales. Numerous ULSMs have been in use with varying degrees of complexity, to represent the urban land surface-atmosphere interactions (Grimmond and et. al., 2010; Masson, 2000; Martilli et al., 2002; Best et al., 2006; Porson et al., 2010a). In the ULSMs with a "tile" approach, the urban areas are treated separately with one or two tiles, with relatively simpler approaches often having the one-tile pattern wherein the urban areas are represented as a flat horizontal surface with bulk thermal and radiative characteristics representative of the impervious urbanized surfaces (Best et al., 2006). More complex models use a two tile approach wherein separate roof and street canyon tiles are used to represent the urban areas and the parameterization of processes based on morphological features with a spatial variability (Masson, 2000; Martilli et al., 2002; Porson et al., 2010a). The Met Office-Reading Urban Surface Exchange Scheme (MORUSES) is the urban-canopy model operationally run in the regional UK Met Office Unified Model since 2016 (UKV NWP model, 1.5-km horizontal resolution over the UK). UKV-MORUSES is based on urban morphology database in London. Previous studies over UK have demonstrated that MORUSES improves surface energy fluxes and near-surface weather (Porson et al., 2010a,b; Bohnenstengel et al., 2011; Bohnenstengel and Hendry, 2016; Hertwig et al., 2020). Simón-Moral et al. (2020) show that MORUSES coupled with the UK Met Office forecast model lead to good performance over Singapore, a tropical city. The implementation of MORUSES results in accurate surface air temperature and wind speed over the urban regions from Seoul Kim et al. (2019). We present here the MORUSES scheme introduced within the high-resolution Delhi Model (DM) using Delhi based urban morphology data. DM is extensively used in National Centre for Medium Range Weather Forecasting (NCMRWF) for research as well as operational forecasts (Jayakumar et al., 2018, 2021).

The present study has the following objectives:

- Evaluate MORUSES with detailed urban representation for Delhi domain against the default one tile scheme, in the simulation of surface energy fluxes and near-surface weather fields.
- Assess the effects of realistic urban morphology data in the simulation of urban processes; comparing a new empirical relationship derived for Delhi with those derived originally from the data for London.
- Study the diurnal evolution of UHI and urban cool island (UCI) characteristics in these new configurations.

The paper is organized as follows, section 2 describes the methodology and section 3 highlights the results, followed by discussion and conclusions in section 4.

2 | METHODOLOGY

A brief description of the atmospheric model, urban parameterization and the numerical experiments are detailed in this section.

2.1 | Model description

The model used for the study is the DM which is a nested limited area model configuration of the Met Office Unified Model (UM). The UM configuration is based on the Regional Atmosphere and Land configuration (RAL1; Bush et al., 2020). Model configuration and science details are already presented in Jayakumar et al. (2018). The Joint UK Land Environment Simulator (JULES) is used to calculate the surface energy balance fluxes between the land surface and the lowest atmospheric level in DM. The configurations of JULES discussed in this paper consist of 9 or 10 tiles depending on the urban energy balance scheme. The surface energy balance fluxes are determined separately for each tile by calculating the corresponding gradients between the surface and the first atmospheric layer. Urban areas are represented in JULES either by a single urban tile (1T) scheme or using a 2-tile (2T) approach that splits the urban surface into a roof and a street canyon. For the 2T approach, JULES has two options: (i) a simple 2T slab scheme (Best et al., 2006) and (ii) the MORUSES scheme (Porson et al., 2010a; Best et al., 2011; Best and Grimmond, 2016).

2.2 | MORUSES in Delhi model with a new empirical relationship

In urban canopy schemes, urban surfaces are simplified to a street canyon, where a road is bordered by two building walls. Buildings are kept along identical roads where the length of the roads are assumed to be far greater than their width (Oke, 1988). In a similar way, MORUSES also assumes the urban areas are two-dimensional infinitely long street canyons consisting of a street canyon tile made up of walls and a street, and a separate roof tile. It is designed to work with the urban morphology input parameters such as building geometry and material properties. Based on these parameters, MORUSES calculates the roughness lengths for momentum and heat, effective albedo, which also accounts for solar zenith angle, effective emissivity and heat capacity used in the surface energy balance as a function of the spatially varying street canyon geometry. The presence of a street canyon in MORUSES allows modelling of radiative fluxes more accurately with short and long wave radiative trapping. Scalar fluxes in MORUSES are computed through a resistance network taking into account three different flow regimes in the street canyons. (Harman et al., 2004; Porson et al., 2010a; Best et al., 2011; Bohnenstengel et al., 2011; Bohnenstengel and Hendry, 2016; Simón-Moral et al., 2020). The road facet of the canyon is conductively coupled to the ground while the roof is radiatively coupled. A detailed description of MORUSES is available in Porson et al. (2010a,b). MORUSES uses morphological input data such as average building height (H), height to street canyon width ratio ($\frac{H}{W}$) and repeating ratio ($\frac{W}{R}$) to describe the geometry of an urban area at each grid point, where W is the street-canyon width and R is the combined length of canyon and roof. These parameters are calculated in the two-dimensional approximation as:

$$\frac{H}{W} = \frac{\pi \lambda_f}{2(1-\lambda_p)} \tag{1}$$

$$\frac{W}{R} = 1 - \lambda_p \tag{2}$$

where λ_f and λ_p are frontal area index and planar area index respectively, and the factor $\frac{\pi}{2}$ arises due to orientational averaging. λ_p is the fraction of the urban tile occupied by buildings and hence $\frac{W}{R}$ is the fraction of non-building surface. λ_f and λ_p are defined as in (Grimmond and Oke, 1999):

$$\lambda_p = \frac{A_p}{A_T} \tag{3}$$

$$\lambda_f = \frac{A_f}{A_T} \tag{4}$$

where A_p, A_f and A_T are plan area of buildings, building frontal area facing the wind in a particular direction, and plan area of total surface, respectively (Bohnenstengel et al., 2011; Bohnenstengel and Hendry, 2016; Simón-Moral et al., 2020). The high-resolution urban morphological ancillaries required for the MORUSES scheme are not available for the whole study domain over Delhi. Bohnenstengel et al. (2011) has derived empirical relationships to generate these input parameters over the whole domain of London which are not covered by the urban morphology data. However, the relationship is derived based on London data and the usefulness of the relationship is not tested outside of London especially over tropics. In addition, the urban geometry such as the building structures are different in Delhi region compared to London. Here, the urban areas lack a well defined pattern having irregular building designs and orientations. Hence new empirical relationships based on the urban morphology data of Delhi are derived as described in sections 2.2.1 and 2.2.2. These empirical relationships are further used to generate urban morphology ancillaries needed for the MORUSES scheme.

Anthropogenic heat flux is considered as an additional heat source term in MORUSES (Bohnenstengel et al., 2011). Anthropogenic heat flux (QF) is estimated in MORUSES scheme using a top-down, energy-consumption inventory method, which was derived based on socioeconomic statistics and energy consumption data for Delhi. The heat released due to electricity consumption, vehicular emissions, fuel consumption in domestic sector and waste heat from power plants are taken into account. Vehicular emissions have been found to be the sector with the largest contribution. The second highest emitting source is electricity consumption followed by domestic fuel consumption and waste heat from power plants (Bhati and Mohan, 2016). The spatially varying field of daily total QF data for the year 2010 is used in the analysis. The QF values are allocated (Annual average in Wm^{-2}) to a spatial fishnet in ArcMap which is proportioned grid wise at 330 m resolution. QF is part of the MORUSES scheme and this local QF data is used in the numerical experiments with MORUSES. The maximum magnitude of annual average of grid mean QF data over the study domain is up to 15 Wm^{-2} . A diurnal profile is also determined and applied in the MORUSES to obtain the diurnal cycle of QF. Since the primary sources are associated with vehicles, the diurnal factor exhibits a bimodal nature with peaking in the morning around 9 am Indian standard time (IST) and evening rush hours around 6 PM IST which is connected to the peak office hours.

2.2.1 | Retrieval of urban morphology data

Urban Morphology data of Delhi region (planar area index, building height and frontal area index) has been retrieved from Very High Resolution (VHR) optical satellite stereo data of Pleiades 1A/1B (0.5 m resolution stereo) (Coeurdevey and Fernandez, 2012). The raw satellite stereo pairs have been pre-processed in Photogrammetric workstation and the accuracy of the model has been improved by ingesting high quality ground control points obtained through Differential Global Positioning System (DGPS) survey (Gupta et al., 2017). The intermediate outputs of Digital Surface Model (DSM), Digital Terrain Model (DTM), Normalised Digital Surface Model (nDSM) and Ortho images have been further processed to obtain the detailed urban morphology data of Delhi (Gupta, 2019). Detailed methodology steps for computation of urban morphology data from VHR optical stereo have been copyrighted under Copyright (Amendment) Act, 2012 of Government of India (Gupta, 2022). Obtained building height layer has been validated against ground observations of building heights and average RMS error found to be 0.3 m (Gupta et al., 2017; Gupta, 2019). Validation of λ_p with ground observations shows accuracy of 85% which is in acceptable limits. λ_f is calculated by employing Urban Morphology Extractor (UME) tool developed at the Indian Institute of Remote Sensing, Dehradun (Jhaldiyal et al., 2018) for prevailing wind direction in winter season namely west direction as the focus of the study was fog prediction. Evaluation of frontal area index computed from UME shows an error of 3% when tested on a sample building datasets (Jhaldiyal et al., 2018).

2.2.2 | Empirical relationship of urban morphology data with urban fraction

Empirical fitting functions are derived for λ_f, λ_p and H using the correlation with urban fraction (fu) and local urban morphology data by employing the method described by Bohnenstengel et al. (2011). Indian Space Research Organization (ISRO) high-resolution land-use land cover (LULC) data are used for deriving fu (*https://www.isro.gov.in/earth-observation/land-use-cover*). Urban morphology data (λ_f, λ_p and H) for Delhi are processed at 30 m resolution from VHR satellite data retrieved at 0.5 m resolution as described in section 2.2.1 and further up scaled to 330 m model resolution using grid average approach (Figure 1). Empirical relationships are established between fu and the input parameters λ_f, λ_p and H as shown in Figure 2. The λ_p is determined as:

$$\lambda_p = 0.6121fu^2 + 0.2179fu + 0.004 \tag{5}$$

The λ_f is defined as

$$\lambda_f = -4.7883fu^6 + 14.447fu^5 - 16.833fu^4 + 9.5361fu^3 - 2.7637fu^2 + 0.4124fu + 0.0014 \tag{6}$$

and finally the H is calculated as

$$H = -58.974fu^6 + 305.3fu^5 - 449.15fu^4 + 252.251fu^3 - 42.235fu^2 + 0.2127fu + 1.5192 \tag{7}$$

The coefficient of determination (R^2) value of λ_p, λ_f and H with fu are 0.87, 0.46 and 0.40 respectively. UME does not count the frontal area of buildings which fall in the shadow of the front building in that particular direction.

Figure 3 displays a comparison between the morphological parameters calculated based on the empirical equations derived for London by Bohnenstengel et al. (2011) (hereafter referred as EMP-LON) and based on the newly derived relationships using Indian data (hereafter referred as EMP-IND) as a function of urban fraction. Further details about EMP-IND and EMP-LON are described together with a schematic (Figure A.3) in Appendix A. EMP-LON generates high values of λ_f, λ_p and H for large magnitudes of urban fractions, which represents taller buildings with narrow street canyons. Whereas lower values of λ_f, λ_p and H are associated with low medium-rise buildings. In the case of EMP-IND, the magnitudes of λ_p are larger compared to EMP-LON for high urban fraction while the λ_f values from EMP-IND are very low and vary less with urban fraction. The morphological parameters from the Indian data indicate high density of urban built up with several small and medium rise building types within the highly urbanized area. Though the λ_f values from the EMP-IND are very low, such small values are reported over cities in U.S. and France (Burian et al., 2003; Sabatino et al., 2010). It should also be noted that the errors in the calculation of may be caused by the irregular orientation, unsymmetrical built environment and wind direction.

Since Climate Change Initiative (CCI) land use land cover data (CCI, 2017) is currently used in DM for research and operational purpose over Delhi, the numerical simulations are carried out using CCI LULC (Figure 4). Though very high-resolution ISRO LULC data is used for the determination of empirical fit, such high-resolution data is yet to be used in the DM model. However we have tested MORUSES with coarse resolution ISRO LULC data which also show performance similar to CCI (not shown). Maximum magnitudes of λ_p for EMP-IND and EMP-LON using CCI LULC are 0.52 and 0.26 respectively, while those of λ_f are 0.03 and 0.17 (See Appendix A for further details). This implies that the urban region in the study domain in both EMP-LON and EMP-IND fall under real cities as mentioned in Grimmond and Oke (1999) while the flow field will be in the wake or isolated regime. Simón-Moral et al. (2020) also reported λ_p up to 0.6 for two- to four-storey buildings and shop houses over Singapore. All the simulations use same radiative and thermal properties across the model

domain by assuming asphalt roads, brick walls and clay roofs as in Bohnenstengel et al. (2011). Majority of the roads in Delhi are asphalt based and the buildings are mostly made of bricks. Since the observations of these parameters are not available over Delhi, further research on the role of urban material properties on MORUSES is beyond the scope of current research. Previous studies have reported the sensitivity of these parameters with MORUSES scheme (Wie et al., 2020; Hertwig et al., 2020).

2.3 | Numerical experiments

Three numerical experiments with a horizontal resolution of 330 m are analyzed in this paper (see Table 1) and all of them are carried out using DM with a one-way nesting approach. The outer 1.5 km model domain spans from 25.16°N to 32.15°N in the meridional direction and from 73.61°E to 80.6°E in the zonal direction. The inner 330 m model domain extends from 28.2°N to 29.1°N in the meridional, and from 76.65°E to 77.55°E in the zonal direction, respectively (Figure 5). There are 80 vertical levels in the inner domain where the first vertical level is at 5 m and 38.5 km is taken as the top of the atmosphere. The simulations use the same model configuration, initialization and physical parameterization except the urban scheme. The first experiment uses the default one tile urban parameterization scheme (Best et al., 2006) and is defined as BEST-1t. In the second experiment, MORUSES-IND, the simulations are conducted using the two tile MORUSES scheme with empirical relation based on Delhi morphology, while the third experiment, MORUSES-LON is based on MORUSES scheme with empirical relation based on Bohnenstengel et al. (2011) (See equation 12, 13 and 14 and Figure A.3 in the Appendix A for further details.). All the numerical simulations start at 0000 UTC using Global UM analysis fields and a forecast is made for 48 h time period. The global UM provides the boundary conditions for the 1.5 km grid-length outer domain which provides the boundary conditions for the 330 m grid-length domain over Delhi (Figure 5).

2.4 | Synoptic situations and observational data

Local weather over the Indian subcontinent is mostly influenced by northeast (during December to March) and southwest (June to September) monsoonal winds. During the winter season, the entire northern India region is often affected by western disturbances (a series of alternate low- and high-pressure systems), which move from west to east, leading to frequent cold waves, haze and fog which further lead to the accumulation of pollutants in the Delhi region (Dimri et al., 2015). The performance of MORUSES is examined on the 9 clear and 11 fog days chosen from November to January between the years 2016 and 2020, representing the winter season. Clear and calm conditions during winter period lead to strong coupling between the surface and atmosphere. The days with visibility greater than 1 km for all the hours are selected for clear case. The days with visibility less than 1 km that persist for more than 3 hours over a 24 hour period are identified for fog cases. Accordingly a total of 11 fog and 9 clear days are selected for the study period. Further details of the case study is seen in Table 2. Surface meteorological observations available from Metar observation data from Indira Gandhi International Airport, referred hereinafter as IGI (77.9 °E, 28.57 °N), New Delhi (Figure 4) is used for verification of screen temperature at 1.5 m (T_{screen}), wind speed at 10 m and relative humidity at 2m. These are analyzed by extracting the corresponding simulation data chosen from the grid points closest to the automatic weather station. Screen-level air temperature simulations are further verified over four different Automatic Weather Station sites over Delhi (Figure 4). These observation sites and the variables are selected based on the data availability and quality checked during the evaluation period. It is to be noted that the three urban sites JR (76.96 °E, 28.68 °N), SD (77.37 °E, 28.68 °N) and PA (77.27 °E, 28.6 8°N) have similar urban fractions of 0.76 in the model due to the homogeneous nature of CCI land surface data. The nearest surroundings of JR is primarily rural, whereas the immediate neighborhoods of the other urban sites including IGI are urbanized. The rural station MT (77.07 °E, 28.88 °N) is chosen in the northern surroundings of the urban area.

Further, the individual components of the surface energy balance equations are examined as defined:

$$Q^* + Q_F = Q_H + Q_{LE} + Q_G + Q_S \tag{8}$$

where Q^* is the sum of the incoming and outgoing radiation components

$$Q^* = K\downarrow - K\uparrow + L\downarrow - L\uparrow . \tag{9}$$

Q_H and Q_{LE} are the sensible and latent heat flux respectively. Q_G represents the ground heat flux and Q_S defines the storage term. Q_F is the anthropogenic flux term. K is the shortwave radiation flux and L is the long wave radiation flux. The observation data for the energy fluxes are obtained over IGI from the Winter Fog Experiment (WIFEX) and include the eddy covariance data and the radiation components. WIFEX is an intensive ground-based measurement over Indo-Gangetic belt initiated by Ministry of Earth Sciences (MoES), which provides an opportunity to evaluate MORUSES at sub-km resolution at IGI (Ghude et al., 2017). Eddy covariance data and radiations fluxes are not available on all the days as mentioned in Table 2 and also data gap is exist during the observation hours in some of the days. Finally on an average four days data are used for the analysis of clear and foggy conditions. Since it will be difficult to differentiate Q_S and Q_G separately, they are included as part of residual and are not considered here. Model performance is evaluated using evaluation metrics including root mean square error (RMSE) and mean bias defined as:

$$RMSE = \sqrt{\frac{\Sigma_{i=1,N}(M_i - O_i)^2}{N}} \tag{10}$$

$$MeanBias = \frac{(M_i - O_i)}{N} \tag{11}$$

where M is model simulation, O is observation and N is the number of data points/hours.

3 | RESULTS

3.1 | Performance of MORUSES scheme

Figure 6 shows the mean diurnal cycle of T_{screen}, wind speed the agreement between model and the observations. The times of maxima and minima as well as the faster evening cooling rates are well reproduced in MORUSES-IND. However, there is still a warm bias during the daytime peak hours that intensifies particularly on day2 up to 2 and 2.3 °C (~ 33 UTC) on clear and fog cases respectively (Figure 6 a and b). Compared to BEST-1t, the RMSE of T_{screen} is reduced by 29% for the clear and fog cases respectively using MORUSES-IND (Table 3). The present results are in good agreement with similar studies reported over London (Bohnenstengel et al., 2011) and Singapore (Simón-Moral et al., 2020).

Wind speed plays an important role in the skin temperature and T_{screen} coupling and thereby in the calculation of T_{screen}. Figure 6 (c-d) display the temporal variations of mean wind speed for clear sky and fog cases respectively. The diurnal cycle of wind speed observations demonstrate that larger wind speeds prevail during clear skies, while calm wind conditions predominate the fog day. It is noteworthy that MORUSES-IND yields remarkable improvement in reproducing the diurnal pattern and magnitude of wind speed except during the afternoon hours for both the clear and fog days. In contrast with BEST-1t, MORUSES-IND causes an increase of mean wind speed up to 2.25 and 1.6 m s^{-1} respectively on clear and fog days. RMSE of wind speed exhibits

an improvement of ~ 15 and 17 % on clear and fog days using MORUSES-IND (Table 3). The performance of MORUSES-LON show slight improvement in the magnitude especially in the evening and night hours on clear sky days though the pattern does not deviate much from the 1 tile scheme. MORUSES-IND cools the T_{screen} more accurately in the evening and at night and increases the magnitudes of wind speed which all exemplify the importance of the reduced urban characteristics, compared to MORUSES-LON over Delhi.

Figure 6 (e-f) shows the diurnal variation of 2-m relative humidity for clear and fog conditions. Overall, a good agreement is found between the observed and predicted magnitudes of relative humidity for clear sky conditions compared to the foggy cases. Among the numerical experiments, MORUSES-IND improves the magnitudes of relative humidity in the evening and night hours. However there exist strong dry bias in the simulation of relative humidity from the three numerical experiments especially during the foggy days. Relative humidity depends on the temperature, and the bias correlates well with the corresponding temperature biases. The warmer and drier condition in the numerical simulations compared to the observation indicate a poor representation of fog in the model which will be further discussed. A recent study by Bharali et al. (2019) have shown that aerosol boundary layer interaction increase near-surface relative humidity by suppressing the vertical extent of the boundary layer and favoring the accumulation of pollutants near the surface. In the present DM model, aerosol interaction is not included and the absence of proper aerosol feed back in the model might be another cause of the dry bias and this aspect will be addressed in future.

Figure 7 shows the mean diurnal cycle of T_{screen} observed and simulated for clear and fog cases respectively over other different locations over Delhi. Here JR, SD and PA are the urban sites and MT is a rural site. Since the observations are not available on all the evaluation days and missing data is present in a few days over some of the sites, ensemble mean of the simulations are calculated only for the period where observations are available. All three simulations reproduce the overall diurnal pattern of T_{screen} reasonably good over all the locations. As expected, the peak values of T_{screen} observed over all the four locations larger for the clear cases in comparison with the foggy events. Similar to IGI, a systematic warm bias is evident during the evening and night hours over the urban locations - JR, SD and PA and the introduction of MORUSES-IND consistently reduces the warm bias during the evening and night hours. Among the numerical experiments, MORUSES-LON increases the warm bias in the night hours and the magnitudes deviates more away from the observations. Detailed statistics are presented in Table 4. Compared to BEST-1t, MORUSES-IND reduces the RMSE of T_{screen} over these locations by 20-23% during the clear cases and upto 13% during the fog conditions. Though MORUSES-IND improves the magnitudes of near surface variables to a reasonable level over the urban locations, RMSE and biases still exist over these sites which are partly due to the inaccuracy in the representation of urban fraction and morphology. Foggy conditions introduce further uncertainties in the surface variables. As expected, there is no difference among the urban schemes over the rural location MT. The bias in the T_{screen} magnitudes over MT during the day time is likely due to the misrepresentation of vegetation. Other factors such as soil conductivity, as seen in Smith et al. (2021) may together with inherent uncertainties of the model, for example aerosols, also result in inaccuracies in the simulations. Overall, the introduction of the MORUSES scheme with the Indian empirical relationships improves and reproduces the urban characteristics such as the impact of buildings and canyons specific to Delhi as mentioned in section 2.2.2. The improved urban characteristics result in a more realistic simulation of T_{screen}, wind speed and relative humidity. The changes in the wind speed are most likely due to the improved roughness length for momentum using the MacDonald parametrisation in the MORUSES scheme (Macdonald et al., 1998).

3.2 | Impact of MORUSES scheme on energy balance fluxes: Study of fog and clear day events

The influence of urban morphology on the surface energy fluxes and their role in the simulation of near-surface variables are studied for clear and foggy days. Figure 8 and 9 illustrate the ensemble mean diurnal cycle of meteorological variables and surface energy fluxes simulated and measured on the clear and fog days respectively at IGI. As mentioned in section 2.4, surface energy fluxes for the fog and clear sky cases are obtained from the WIFEX measurements. The latent heat flux observations

for the foggy conditions and the measurements of T_{skin} for both conditions are not available during the study period. For the surface energy balances, the evaluation focuses on the radiation terms Q^*, net short wave radiation $Q_K(K\downarrow - K\uparrow)$, net long wave radiation, $Q_L(L\downarrow - L\uparrow)$, Q_H and Q_{LE}.

On the clear cases, modelled and observed Q^* are in good agreement except in the evening and night hours. It is to be noted that the Q_K and Q_L are in opposite direction with positive and negative values respectively. Hence, the Q^*, the net effect of Q_K and Q_L shows less bias though Q_K and Q_L have large bias individually and also the Q^* is dominated by the larger magnitude of Q_K during the day (Hertwig et al., 2020). Q^* from the three experiments are similar except during the daytime peak hours where MORUSES produces a larger Q^* compared to BEST-1t. Q_K has a higher daytime peak in MORUSES than in the BEST-1t simulations. This is partly a consequence of the lower albedo in the canyon component of MORUSES resulting in an increase in the net short wave radiation (Bohnenstengel and Hendry, 2016). Q^* has a negative bias during the sunset hours which arises from the bias in the Q_L. The simulations of Q_L deviate away from the observations in terms of magnitude and phase. Though the introduction of MORUSES-IND improves the magnitudes of Q_L to some extent, there still exist significant bias. In order to understand the discrepancy, the components of Q_L, $L\downarrow$ and $L\uparrow$ are further examined. The magnitude and phase of $L\uparrow$ are better predicted via MORUSES-IND in comparison with the observations indicating an improved skin temperature. Comparing the schemes, the magnitudes of $L\uparrow$ from MORUSES-IND are closer to the observations during the daytime while BEST-1t overestimates. This decrease of $L\uparrow$ during the day in MORUSES-IND is correlated with T_{skin} in turn indicating the storage of more heat in the urban fabric. The bias in Q_L mainly comes from the $L\downarrow$ simulation where all three experiments underestimate the incoming long wave radiation. The underestimation of $L\downarrow$ is reported in clear skies, including pre-fog conditions (Wild et al., 2001; van der Velde et al., 2010; Steeneveld and de Bode, 2018). In the present study, the bias in $L\downarrow$ is likely partially caused by the representation of aerosol radiative effects. The UM uses a aerosol climatology from Bush et al. (2019). The aerosol optical depth has increased over northern India since 2000 (Babu et al., 2013) and thus this difference will be contributing to errors in the radiation balance. A more complex aerosol parameterization scheme, such as that used in DM-Chem (Jayakumar et al., 2021), has been shown to improve fog simulations. The daytime peak value of both Q_L and Q_H exhibit a phase delay of ~ 1 hour in BEST-1t compared to MORUSES-IND caused by lower thermal inertia resulting from the inclusion of roof component of MORUSES. The different heat capacities for canyon and roof in MORUSES allow large differences in thermal inertia, thus the roof responds more rapidly to the incoming solar radiation (Hertwig et al., 2020). The difference between the BEST-1t and MORUSES-IND schemes are seen most clearly in the simulated variables during the afternoon and evening hours. Modelled Q_H using MORUSES schemes agree better with the observations where the MORUSES-IND runs capture the phase of Q_H better than MORUSES-LON. In comparison with MORUSES-IND, MORUSES-LON produces relatively higher magnitudes of Q_L, Q_H and T_{skin} during the night hours. High values of the H/W and W/R in MORUSES-LON (Figure A.2) result in a phase delay and reduced diurnal variability compared to MORUSES-IND (Figure 8). The magnitudes of Q_{LE} simulated from the three experiments did not show a larger difference and they are strongly underestimated during the day. Since there is no availability of water from rainfall during the study period, the model cannot simulate a flux of moisture due to evaporation from the urban tile surface but only from either the vegetation or bare soil. So, the possible factors for the present bias are the urban vegetation or the dry soil at IGI with less moisture availability leading to the partition of more Q_H and less Q_{LE}. This can be improved by better representation of urban vegetation through improved LULC and by the inclusion of urban irrigation or any anthropogenic moisture sources (Ao et al., 2018; Dou et al., 2019). Studies have reported that small fraction of vegetation in urban areas could result into significant impact on the local surface energy balance (Best and Grimmond, 2016; Hertwig et al., 2021).

Compared to the clear condition, the impact of MORUSES-IND is more pronounced during the foggy events (Figure 9) consistent with the verification analysis in section 3.1. The simulated variables exhibit a larger difference between BEST-1t and MORUSES-IND over a longer duration (up to 20 hours) on the fog cases. One factor is the relatively low wind speeds on the fog day which increases the local impact of the surface energy balance on near-surface variables compared to the windier conditions seen on the clear days. MORUSES-IND captures the observations more accurately, especially during the evening

and night hours when the urban impact intensifies over the domain. It also simulates the morning and evening transitions more accurately compared to the other two configurations. Modelled Q^* is under-estimated in all simulations during the night time. Compared to the clear sky, the night time Q^* bias is larger in the foggy conditions. Further to that, Q_K exhibit a clear positive bias during the daytime peak hours. Simulated Q_L shows strong over estimation which arise from both $L\downarrow$ and $L\uparrow$. This is in contrast to the clear case where the biases are comparatively smaller and they are mainly from the $L\downarrow$. Along with the other possible factors, the misrepresentation of the fog together with the absence of detailed aerosol chemistry make the bias of Q_L more intense on the foggy cases. Comparing the schemes, MORUSES-IND reduces the overestimation of $L\uparrow$ to a reasonable level, but such impact is not visible for $L\downarrow$. The underestimation of $L\downarrow$ is not unique to the UM for a WIFEX case with a similar bias found in the Weather Forecasting and Research (WRF) model (Pithani et al., 2019). The impact of fog on $L\downarrow$ is discussed further in section 4. MORUSES-IND appears to capture the magnitudes of Q_H more realistically during the sun rise hours. T_{skin} displays more than 5°C difference between MORUSES-IND and BEST-1t during the daytime peak. Further analysis reveals that the weak surface coupling during the daytime when Q_H is large reduces the impact of T_{skin} in the diagnosis of T_{screen}. Although observations of latent heat flux for the foggy conditions were not available from WIFEX, comparison of the numerical simulations showed little difference in Q_{LE}. In summary, the magnitudes of some surface fluxes such as net long wave radiation, latent heat flux are under-estimated in all the simulations though MORUSES-IND leads to slight improvements. The net long wave bias is more significant during the foggy conditions. The differences between the simulations seen at IGI are consistent with those seen over the whole urban area (for details see Appendix B).

3.3 | The urban heat and cool island characteristics

It is well-known that UHI effect manifests as the temperature rise in the built environment relative to the surrounding natural environment. Similarly, some cities in arid and semi-arid regions have been found to exhibit lower surface temperatures than its surrounding rural areas which has been termed as the Urban Cool Island (UCI). The presence of UCI in cities has been reported during certain times of the day or particular season (Rasul et al., 2015; Yang et al., 2017; Mohan et al., 2020). Here the UHI and UCI effects are examined using T_{screen}. Figure 10 a and b illustrate mean diurnal cycle of ΔT_{screen} for clear and fog cases respectively. Here ΔT_{screen} is defined as the difference in T_{screen} between IGI, an urban site, and MT, a rural site. If the magnitude of delta is positive/negative, it is termed as UHI/UCI. Since the ΔT_{skin} observation is not available, it is not depicted. Here, UCI is observed on clear sky conditions during both day1 and day2. Neglecting the fluctuations in the night time, the duration of UCI is around 3 hours between 3 to 6 UTC on both day1 and day2. The results are consistent with the studies by Gupta et al. (2021) using Weather Research and Forecasting model simulations over Delhi region in summer and winter season. Their studies also report UCI effect between 3 to 6 UTC and strong UHI effect during evening and nocturnal hours. The maximum intensity of UCI observation in the present case is ~ 3 °C on the day1 and it is up to ~ 5 °C on the day2. The DM also reproduced the UCI features on the clear conditions on both days where the intensity of UCI reaches up to ~ 5 and 3.9 °C respectively using BEST-1t and MORUSES-IND. Except the peak value of day2, BEST-1t overestimates the magnitudes of UCI and the introduction of MORUSES-IND reproduces the magnitudes of UCI closer to the observations. Compared to the observation, all three numerical experiments simulated the UCI for longer duration, ~ 6 hour. The peak magnitudes of observed UHI ranges from 2-3 °C for clear sky conditions during day1 and day2. he magnitudes of UHI observation show large fluctuations and the values are fluctuates around zero mainly during 15 to 27 hours. It may be noted that the mean variation of T_{screen} obtained from the rural location MT also shows large variability (Figure 7g) during that time interval, which arises due to missing data during some of the clear sky cases. Further examination is not possible due to the absence of continuous data at other rural locations. MORUSES-IND reproduces UHI more closely to the observations while BEST-1t and MORUSES-LON overestimates the magnitudes. There is no UCI observed on the foggy conditions and the UHI is persistent for majority of the time with the magnitudes around ~ 2 °C having less diurnal variability compared to the clear sky cases. In contrast to this, the

DM simulates diurnal variability, producing an UCI and strong UHI characteristics. Compared to BEST-1t and MORUSES-LON, MORUSES-IND has a reduced diurnal variability. All three simulations of T_{screen} for clear and fog cases display a clear UCI during the daytime up to ~ 10 UTC. After this, the UHI forms over the location with a sudden sharp increase of 4-7 ^{o}C in ΔT_{screen}. All three experiments simulate intense UHI in the evening and nocturnal hours, in contrast to a daytime UCI. The intensity of the simulated UHI is stronger than UCI in terms of magnitude and duration. The peak values of UHI is largest in the BEST-1t and UHI undergoes a sharp decrease over night. Whereas UHI from both MORUSES-IND and MORUSES-LON undergo gradual change.

The presence of UCI is attributed to the intense heat storage capacity and the reduced solar radiation gain of high density urban surfaces in the early morning hours (Yang et al., 2017). However during the foggy environment, the amount of solar radiation gain may be lower and reflected radiation from the fog diminishes the radiative cooling both in urban and rural areas, thereby limit the probability of UCI effect (Oke, 1987). On foggy conditions, Jayakumar et al. (2021) has reported a slight surface warming over Delhi in the early morning hours during the initiation phase of fog due to aerosol effect. The exact reason behind the absence of UCI effect during the foggy events have to be explored further.

4 | DISCUSSION AND CONCLUSION

To mitigate the social and economic impacts of fog and other extreme weather event over Delhi, a realistic city scale weather forecast is essential. Since city scale models have a high sensitivity to surface-atmospheric interaction, a detailed representation of urban processes is vital for improving performance. In this study, a more detailed urban surface flux scheme is implemented in a high-resolution regional model, the Delhi Model (Jayakumar et al., 2018), during winter season over Delhi. Three numerical experiments are carried out namely MORUSES-IND, MORUSES-LON and BEST-1t. Both MORUSES-IND and MORUSES-LON use the more detailed two tile urban parameterization scheme MORUSES and the BEST-1t includes a simpler one tile scheme. The urban morphology data, used in MORUSES is from a newly derived set of empirical relationships (EMP-IND) for the study area in the MORUSES-IND whereas the empirical fit (EMP-LON) based on Bohnenstengel et al. (2011) is used in the MORUSES-LON. The magnitudes of urban morphology index parameters, $\frac{H}{W}$ and $\frac{W}{R}$, generated using EMP-IND are lower compared to that of EMP-LON, which highlights the difference in the built environment between both cities. EMP-LON indicates high rise buildings with narrow canyons over the city center. On the other hand, EMP-IND indicates small sized wide spread buildings over the urban area which realistically represents the development pattern existing in study area. A spatially varying locally derived Q_F with diurnal cycle is also input to the model. An effort has been made to generate the ensemble of simulation for robust results. The major outcomes of the study are highlighted below:

- Wind speed simulated using MORUSES-IND shows an increase in magnitude (25%) compared to BEST-1t and exhibits remarkable improvement in terms of magnitude and phase in day1 and day2 during clear and foggy events at IGI.
- MORUSES-IND reduces the warm bias present in the simulation of T_{screen} using BEST-1t and reproduces the magnitudes more realistically, particularly in the evening and nocturnal hours for both clear and foggy conditions.
- The RMSE of T_{screen} simulated using MORUSES-IND are reduced by 30% and 27 % respectively for clear and fog cases at IGI, compared to BEST-1t while RMSE of wind speed exhibits an improvement of 15 and 17 % on clear and fog days using MORUSES-IND.
- Compared to the clear day, the impact of MORUSES-IND is more pronounced on the foggy day.
- BEST-1t delays the daytime peak of Q_L and Q_H on the fog day, whilst the phase delay and the magnitudes are found to be close to the observational values for MORUSES-IND.
- All three experiments show co-existence of UHI/UCI phenomena with strong UHI characteristics in the evening and night

time while a weaker UCI effect on the morning hours between 3 to 9 UTC for the clear sky and foggy conditions. But the UCI effect is observed only for the clear sky cases and the duration is around 3 hours.

- In comparison with MORUSES-LON and BEST-1t, MORUSES-IND minimizes the intensity of both the UCI and UHI effect for the clear sky and foggy conditions.

The large biases in the simulation of relative humidity especially during the foggy conditions and the underestimation of Q_{LE} in all the three configurations for the foggy conditions are some of the important issues reported in the current study. The inclusion of hydrological processes such as urban irrigation or any anthropogenic moisture sources in MORUSES will provide an opportunity to explore their impacts. Since the percentage of vegetation controls the partitioning of Q_{LE} and Q_H, better representation of subgrid scale urban vegetation variability through high resolution LULC is another potential area for the improved model performance. Currently the empirical relationships are used for the generation of urban morphology which are simple and easy to use. In future, ingestion of original urban morphology data in mosaic mode will be experimented for improved results.

Another important aspect is the bias in the magnitudes of Q_L, particularly in $L_{\downarrow}$ in all the three configurations which is partly due to the underestimation of fog in the model. Early dissipation and daytime persistence of fog is a known issue in the UM (Smith et al., 2021). Though accurate simulations of fog is a big challenge due to the complex feedback between different processes such as boundary layer turbulence, cloud micro-physics and radiative cooling. In this regard, one of the powerful tool is to drive the land surface model, JULES offline by observations, hence remove the feedback from the fog and other atmospheric processes. This would pick apart the differences in performance, which is purely from the surface. Regarding fog representation, an appropriate micro-physics scheme for the location is essential for capturing the optical depth, and associated increase in $L_{\downarrow}$, of fog (Müller et al., 2010; Boutle et al., 2018; Poku et al., 2019; Ducongé et al., 2020). Boutle et al. (2018) found that a reduced droplet number concentration near the surface produced fog which was physically more consistent with observations of fog in the UK. A small set of sensitivity experiments, removing the adjustment to the near-surface droplet number concentration, introduced by Boutle et al. (2018), reproduced the fog optical depth closer to the WIFEX observations but biases in $L_{\downarrow}$ remain. Further research is needed to aid model development and improve fog simulations.

Another limitation of the current study is the lack of urban aerosol and associated processes within the boundary layer in the model. During the winter period, polluted regions like Delhi accumulate large aerosol concentrations within the shallow boundary layer, in turn intensifying fog development (Duynkerke, 1991). Poku et al. (2019) and Poku et al. (2021) have demonstrated that the treatment of aerosol activation and aerosol-fog interactions are critical for accurate fog simulations. Recent work by Jayakumar et al. (2021) have introduced DM with the reduced version of the UK Chemistry and Aerosol model (UKCA; Mulcahy et al., 2020), called DM-Chem, which couples aerosols and clouds explicitly. Merging MORUSES to this configuration of the model is planned in near future. This way a more realistic representation of the two way feedback between aerosol emissions and urbanisation will be employed, which will ultimately aid the mitigation policies over tropical cities like Delhi.

5 | ACKNOWLEDGEMENTS

This work was conducted through the "Weather and Climate Science for Service Partnership India" (WCSSP)-India, a collaborative initiative between the Indian Ministry of Earth Sciences (MoES) and the Met Office, supported by the UK Government's Newton Fund. The authors would like to thank Huw Lewis and Sylvia Bohnenstengel for scientific discussions. Observational data for the fog day are obtained as part of winter fog experiment (WIFEX) campaign conducted in collaboration with MoES, the Indian Institute of Tropical Meteorology and India Meteorological Department

REFERENCES

Ao, X., Grimmond, C. S. B., Ward, H. C., Gabey, A. M., Tan, J., Yang, X.-Q., Liu, D., Zhi, X., Liu, H., Zhang, N., 2018. Evaluation of the surface urban energy and water balance scheme (suews) at a dense urban site in shanghai: Sensitivity to anthropogenic heat and irrigation. Journal of Hydrometeorology 19 (12), 1983 – 2005.
URL https://journals.ametsoc.org/view/journals/hydr/19/12/jhm-d-18-0057_1.xml

Babu, S. S., Manoj, M. R., Moorthy, K. K., Gogoi, M. M., Nair, V. S., Kompalli, S. K., Satheesh, S. K., Niranjan, K., Ramagopal, K., Bhuyan, P. K., Singh, D., 2013. Trends in aerosol optical depth over indian region: Potential causes and impact indicators. Journal of Geophysical Research: Atmospheres 118 (20), 11,794–11,806.
URL https://agupubs.onlinelibrary.wiley.com/doi/abs/10.1002/2013JD020507

Best, M. J., Grimmond, C. S. B., 2016. Modeling the Partitioning of Turbulent Fluxes at Urban Sites with Varying Vegetation Cover. J. of hydromet. 17, 2537–2553.

Best, M. J., Grimmond, C. S. B., Villani, M., 2006. Evaluation of the Urban Tile in MOSES using Surface Energy Balance Observations. Boundary-Layer Meteorol 118, 503–525.

Best, M. J., Pryor, M., Clark, D. B., Rooney, G. G., Essery, R. L. H., Ménard, C. B., Edwards, J. M., Hendry, M. A., Porson, A., Gedney, N., Mercado, L. M., Sitch, S., Blyth, E., Boucher, O., Cox, P. M., Grimmond, C. S. B., Harding, R. J., 2011. The joint uk land environment simulator (jules), model description – part 1: Energy and water fluxes. Geoscientific Model Development 4 (3), 677–699.
URL https://gmd.copernicus.org/articles/4/677/2011/

Bharali, C., Nair, V. S., Chutia, L., Babu, S. S., 2019. Modeling of the effects of wintertime aerosols on boundary layer properties over the indo gangetic plain. Journal of Geophysical Research: Atmospheres 124 (7), 4141–4157.
URL https://agupubs.onlinelibrary.wiley.com/doi/abs/10.1029/2018JD029758

Bhati, S., Mohan, M., 2016. Estimation of anthropogenic heat emissions in delhi, india and their role in urban heat island effect. Proceedings of the AGU Fall Meeting Abstracts 2016, B43I–06.

Bohnenstengel, S., Evans, S., Clark, P., Belcher, S., 2011. Simulations of the London urban heat island. Q. J. R. Meteorol. Soc. 137, 1625–1640.

Bohnenstengel, S., Hendry, M., 2016. Report on implementation and evaluation of moruses in the ukv ps37. Report.
URL https://digital.nmla.metoffice.gov.uk/IO$_$30a48cac-662d-48ce-9a63-f5e81496c665/

Boutle, I., Price, J., Kudzotsa, I., Kokkola, H., Romakkaniemi, S., 2018. Aerosol–fog interaction and the transition to well-mixed radiation fog. Atmospheric Chemistry and Physics 18 (11), 7827–7840.
URL https://www.atmos-chem-phys.net/18/7827/2018/

Burian, S. J., Han, W. S., Brown, M. J., 2003. Morphological Analyses Using 3D Building Databases: Houston, Texas. Report.
URL https://www.researchgate.net/publication/260339606

Bush, M., Allen, T., Bain, C., Boutle, I., Edwards, J., Finnenkoetter, A., Franklin, C., Hanley, K., Lean, H., Lock, A., Manners, J., Mittermaier, M., Morcrette, C., North, R., Petch, J., Short, C., Vosper, S., Walters, D., Webster, S., Weeks, M., Wilkinson, J., Wood, N., Zerroukat, M., 2020. The first met office unified model–jules regional atmosphere and land configuration, ral1. Geoscientific Model Development 13 (4), 1999–2029.
URL https://gmd.copernicus.org/articles/13/1999/2020/

Bush, M., Allen, T., Bain, C., Boutle, I., Edwards, J., Finnenkoetter, A., Franklin, C., Hanley, K., Lean, H., Lock, A., Manners, J., Mittermaier, M., Morcrette, C., North, R., Petch, J., Short, C., Vosper, S., Walters, D., Webster, S., Zerroukat, M., 06 2019. The first met office unified model/jules regional atmosphere and land configuration, ral1. Geoscientific Model Development Discussions, 1–47.

CCI, 2017. Esa. land cover cci product user guide version 2. Tech. Rep.
URL http://maps.elie.ucl.ac.be/CCI/viewer/download/ESACCI-LC-Ph2-PUGv2_2.0.pdf

Coeurdevey, L., Fernandez, K., 2012. Defence and space intelligence pléiades imagery user guide.
URL https://www.intelligence-airbusds.com/automne/api/docs/v1.0/document/download/ZG9jdXRoZXF1ZS1kb2N1bWVudC01NTY0Mw==/ZG9jdXRoZXF1ZS1maWxlLTU1NjQy/airbus-pleiades-imagery-user-guide-15042021.pdf

Dimri, A. P., Niyogi, D., Barros, A. P., Ridley, J., Mohanty, U. C., Yasunari, T., Sikka, D. R., 2015. Western disturbances: A review. Reviews of Geophysics 53 (2), 225–246.
URL https://agupubs.onlinelibrary.wiley.com/doi/abs/10.1002/2014RG000460

Dou, J., Grimmond, S., Cheng, Z., Miao, S., Feng, D., Liao, M., 2019. Summertime surface energy balance fluxes at two beijing sites. International Journal of Climatology 39 (5), 2793–2810.
URL https://rmets.onlinelibrary.wiley.com/doi/abs/10.1002/joc.5989

Ducongé, L., Lac, C., Vié, B., Bergot, T., Price, J. D., 2020. Fog in heterogeneous environments: the relative importance of local and non-local processes on radiative-advective fog formation. Quarterly Journal of the Royal Meteorological Society 146 (731), 2522–2546.
URL https://rmets.onlinelibrary.wiley.com/doi/abs/10.1002/qj.3783

Duynkerke, P. G., 1991. Radiation fog: A comparison of model simulation with detailed observations. Monthly Weather Review 119 (2), 324 – 341.
URL https://journals.ametsoc.org/view/journals/mwre/119/2/1520-0493$_$1991$_$119$_$0324$_$rfacom$_$2$_$0$_$co$_$2.xml

Gautam, R., Singh, M. K., 2018. Urban heat island over delhi punches holes in widespread fog in the indo-gangetic plains. Geophysical Research Letters 45 (2), 1114–1121.
URL https://agupubs.onlinelibrary.wiley.com/doi/abs/10.1002/2017GL076794

Ghude, S., G. S. Bhat, G. S., Prabhakaran, T., Jenamani, R. K., Chate, D. M., Safai, P. D., Rajeevan, M., et.al, 2017. Winter fog experiment over the Indo-Gangetic plains of India. Curr. Sci. 112, 767–784.

Grimmond, C. S. B., et. al., 2010. Multi-year energy balance and carbon dioxide fluxes over a residential neighbourhood in a tropical city. J. Appl. Meteor. Climatol 49, 1268–1292.

Grimmond, C. S. B., Oke, T. R., 1999. Aerodynamic Properties of Urban Areas Derived from Analysis of Surface Form. J. Appl. Meteor. 38, 1262–1291.

Gupta, K., 2019. Characterization of urban canopy parameters and its relationship with spatially variable urban climate indicators in complex urban environment. PhD Thesis, Indian Institute of Technology, Roorkee , India.

Gupta, K., 2022. Retrieval of urban canopy parameters from very high resolution optical stereo and multi-spectral data. L-113996/2022.

Gupta, K., Pushplata, Arijit, R., 2021. Assessment of spatio-temporal and diurnal urban heat island intensities in delhi urban agglomeration using a high resolution weather research and forecasting model. American Geophysical Fall Meeting 2021.
URL https://www.researchgate.net/publication/358164537_Assessment_of_Spatio-Temporal_and_diurnal_Urban_Heat_Island_Intensities_in_Delhi_Urban_agglomeration_using_a_high_resolution_Weather_Research_and_Forecasting_Model

Gupta, K., Pushplata, John, S., Bhardwaj, A., Kumar, P., Kumar, A., 2017. Comparative evaluation of pleiades, cartosat- 2 and kompsat-3 stereo data for dsm and 3d model generation. Asian Conference on Remote Sensing, Delhi, India,.
URL https://a-a-r-s.org/proceeding/ACRS2017/Missing_Proceedings/1388.pdf

Harman, I., Barlow, J., Belcher, S., 2004. Scalar Fluxes from Urban Street Canyons Part II: Model. Boundary-Layer Meteorol 113, 387–410.

Hertwig, D., Grimmond, S., Hendry, M., Saunders, B., Wang, Z., Jeoffrion, M., Vidale, P. L., McGuire, P. C., Bohnenstengel, S. I., Ward, H. C., Kotthaus, S., 2020. Urban signals in high-resolution weather and climate simulations: role of urban land-surface characterisation. Theor Appl Climatol 142, 701–728.

Hertwig, D., Ng, M., Grimmond, S., Vidale, P. L., McGuire, P. C., 2021. High-resolution global climate simulations: Representation of cities. International Journal of Climatology 41 (5), 3266–3285.
URL https://rmets.onlinelibrary.wiley.com/doi/abs/10.1002/joc.7018

Jayakumar, A., Gordon, H., Francis, T., Hill, A. A., Mohandas, S., Sandeepan, B. S., Mitra, A. K., Beig, G., 2021. Delhi model with chemistry and aerosol framework (dm-chem) for high-resolution fog forecasting. Quarterly Journal of the Royal Meteorological Society 147 (741), 3957–3978.
URL https://rmets.onlinelibrary.wiley.com/doi/abs/10.1002/qj.4163

Jayakumar, A., Rajagopal, E. N., Boutle, I. A., George, J. P., Mohandas, S., Webster, S., Aditi, S., 2018. An operational fog prediction system for Delhi using the 330 m Unified Model. Atmos. Sci. Lett. 19, 1–7.

Jayakumar, A., Sethunadh, J., Francis, T., Mohandas, S., Rajagopal, E. N., 2019. Impact of Cartosat-1 orography in 330 m Unified Model forecast. Curr. Sci. 116, 816–822.

Jenamani, R. K., 2007. Alarming rise in fog and pollution causing a fall in maximum temperature over delhi. Current Science (00113891) 93 (3).

Jenamani, R. K., 2012. Development of intensity based fog climatological information system (daily and hourly) at IGI airport, New Delhi for use in fog forecasting and aviation. Mausam 63, 89–112.

Jhaldiyal, A., Gupta, K., Gupta, P. K., Thakur, P., Kumar, P., 2018. Urban morphology extractor: A spatial tool for characterizing urban morphology. Urban Climate 24, 237–246.
URL https://www.sciencedirect.com/science/article/pii/S2212095518300993

Kim, D., Hong, S., Byon, J. Y., Park, H., Ha, J. C., 2019. Development and evaluation of urban canopy model based on unified model input data using urban building information data in seoul. Atmosphere 29 (4), 417–427.

Macdonald, R., Griffiths, R., Hall, D., 1998. An improved method for the estimation of surface roughness of obstacle arrays. Atmospheric Environment 32 (11), 1857–1864.
URL https://www.sciencedirect.com/science/article/pii/S1352231097004032

Martilli, A., A, A. C., Rotach, M., 2002. An urban surface exchange parameterisation for mesoscale models. Boundary-Layer Meteorol 104(2), 261–304.

Masson, V., 2000. A physically-based scheme for the urban energy budget in atmospheric models. Boundary-Layer Meteorol 94 (3), 357–397.

Mohan, M., Payra, S., 2009. Influence of aerosol spectrum and air pollutants on fog formation in urban environment of megacity delhi, india. Environ Monit Assess 151, 265–277.

Mohan, M., Sati, A. P., Bhati, S., 2020. Urban sprawl during five decadal period over national capital region of india: Impact on urban heat island and thermal comfort. Urban Climate 33, 100647.
URL https://www.sciencedirect.com/science/article/pii/S2212095519303670

Mulcahy, J. P., Jones, C., Povey, C. G., et. al., 2020. Description and evaluation of aerosol in UKESM1 and HadGEM3-GC3.1 CMIP6 historical simulations. Geosci. Model Dev. 13, 6383–6423.

Müller, M. D., Masbou, M., Bott, A., 2010. Three-dimensional fog forecasting in complex terrain. Quarterly Journal of the Royal Meteorological Society 136 (653), 2189–2202.
URL https://rmets.onlinelibrary.wiley.com/doi/abs/10.1002/qj.705

Oke, T., 1988. Street design and urban canopy layer climate. Energy and Buildings 11 (1), 103–113.
URL https://www.sciencedirect.com/science/article/pii/0378778888900266

Oke, T. R., 1987. Boundary Layer Climates, 2nd Edition. Halsted Press, New York.

Pithani, P., Ghude, S. D., Chennu, V. N., Kulkarni, R. G., Steeneveld, G., Sharma, A., Prabhakaran, T., Chate, D. M., Gultepe, I., Jenamani, R. K., et al., 2019. Wrf model prediction of a dense fog event occurred during the winter fog experiment (wifex). Pure and Applied Geophysics 176 (4), 1827–1846.

Poku, C., Ross, A. N., Blyth, A. M., Hill, A. A., Price, J. D., 2019. How important are aerosol-fog interactions for the successful modelling of nocturnal radiation fog? Weather 74 (7), 237–243.
URL https://rmets.onlinelibrary.wiley.com/doi/abs/10.1002/wea.3503

Poku, C., Ross, A. N., Hill, A. A., Blyth, A. M., Shipway, B., 2021. Is a more physical representation of aerosol activation needed for simulations of fog? Atmospheric Chemistry and Physics 21 (9), 7271–7292.
URL https://acp.copernicus.org/articles/21/7271/2021/

Porson, A., Clark, P., Harman, I. N., MJ, M. B., Belcher, S., 2010a. Implementation of a new urban energy budget scheme in the MetUM. Part I: Description and idealized simulations. Q. J. R. Meteorol. Soc. 136, 1514–1529.

Porson, A., Clark, P., Harman, I. N., MJ, M. B., Belcher, S., 2010b. Implementation of a new urban energy budget scheme into MetUM. Part II: Validation against observations and model intercomparison. Q. J. R. Meteorol. Soc. 136, 1530–1542.

Rasul, A., Balzter, H., Smith, C., 2015. Spatial variation of the daytime surface urban cool island during the dry season in erbil, iraqi kurdistan, from landsat 8. Urban Climate 14, 176–186, cooling Heat Islands.
URL https://www.sciencedirect.com/science/article/pii/S2212095515300237

Roth, M., Jansson, C., Velasco, E., 2017. Multi-year energy balance and carbon dioxide fluxes over a residential neighbourhood in a tropical city. Int. J. Climatol. 37, 2679–2698.

Sabatino, S. D., Leo, L. S., Cataldo, R., Ratti, C. F., Britter, R. E., 2010. Construction of Digital Elevation Models for a Southern European City and a Comparative Morphological Analysis with respect to Northern European and North American Cities. . J. Appl. Meteor. Climatol 49, 1377–1396.

Sati, A. P., Mohan, M., 2021. Impact of urban sprawls on thunderstorm episodes: Assessment using wrf model over central-national capital region of india. Urban Climate 37, 100869.
URL https://www.sciencedirect.com/science/article/pii/S2212095521000997

Simón-Moral, A., Dipankar, A., Roth, M., Sánchez, C., Velasco, E., Huang, X.-Y., 2020. Application of moruses single-layer urban canopy model in a tropical city: Results from singapore. Quarterly Journal of the Royal Meteorological Society 146 (727), 576–597.
URL https://rmets.onlinelibrary.wiley.com/doi/abs/10.1002/qj.3694

Smith, D. K., Renfrew, I. A., Dorling, S. R., Price, J. D., Boutle, I. A., 2021. Sub-km scale numerical weather prediction model simulations of radiation fog. Quarterly Journal of the Royal Meteorological Society 147 (735), 746–763.
URL https://rmets.onlinelibrary.wiley.com/doi/abs/10.1002/qj.3943

Steeneveld, G., de Bode, M., 2018. Unravelling the relative roles of physical processes in modelling the life cycle of a warm radiation fog. Quarterly Journal of the Royal Meteorological Society 144 (714), 1539–1554.

Steeneveld, G. J., Ronda, R. J., Holtslag, A. A. M., 2015. The challenge of forecasting the onset and development of radiation fog using mesoscale atmospheric models. Boundary-Layer Meteorology 154 (2), 265–289.

Syed, F. S., Körnich, H., Tjernström, M., 2012. On the fog variability over south asia. Climate dynamics 39 (12), 2993–3005.

United Nations, 2018. World Urbanization Prospects: The 2018 Revision, Key Facts 2.

van der Velde, I. R., Steeneveld, G. J., Wichers Schreur, B. G. J., Holtslag, A. A. M., 11 2010. Modeling and forecasting the onset and duration of severe radiation fog under frost conditions. Monthly Weather Review 138 (11), 4237–4253.

Wærsted, E. G., Haeffelin, M., Steeneveld, G. J., Dupont, J. C., 2019. Understanding the dissipation of continental fog by analysing the lwp budget using idealized les and in situ observations. Quarterly Journal of the Royal Meteorological Society 145 (719), 784–804.

Wie, J., Hong, S.-O., Byon, J.-Y., Ha, J.-C., Moon, B.-K., 01 2020. Sensitivity analysis of surface energy budget to albedo parameters in seoul metropolitan area using the unified model. Atmosphere 11, 120.

Wild, M., Ohmura, A., Gilgen, H., Morcrette, J.-J., Slingo, A., 2001. Evaluation of downward longwave radiation in general circulation models. Journal of Climate 14 (15), 3227 – 3239.

Yan, S., Zhu, B., Huang, Y., Zhu, J., Kang, H., Lu, C., Zhu, T., 2020. To what extents do urbanization and air pollution affect fog? Atmospheric Chemistry and Physics 20 (9), 5559–5572.
URL https://acp.copernicus.org/articles/20/5559/2020/

Yang, X., Li, Y., Luo, Z., Chan, P. W., 2017. The urban cool island phenomenon in a high-rise high-density city and its mechanisms. International Journal of Climatology 37 (2), 890–904.
URL https://rmets.onlinelibrary.wiley.com/doi/abs/10.1002/joc.4747

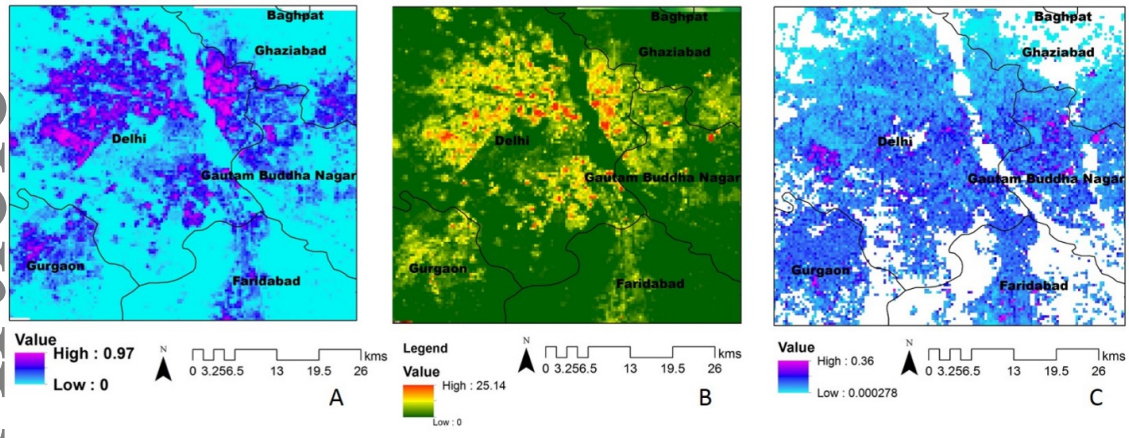

FIGURE 1 Urban morphology parameters (a) planar area index (b) building height and (c) frontal area index as a function of urban fraction derived from ISRO high-resolution LULC data

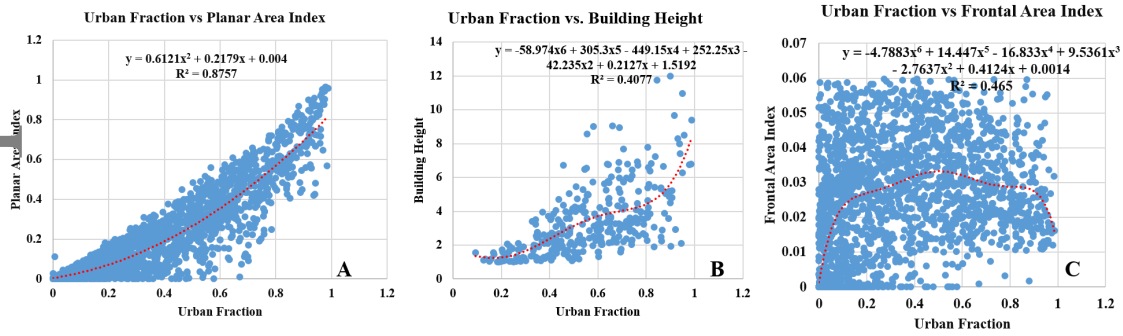

FIGURE 2 Empirical fit relationships (a) planar area index (b) building height and (c) frontal area index as a function of urban fraction derived from ISRO high-resolution LULC data

.1 | Appendix A

Figure A.1 shows urban morphology parameters, λ_f, λ_p and H using CCI data for EMP-IND and EMP-LON. Associated morphology index are plotted in Figure A.2. The mean building height, H values are low (4.24 m) in EMP-IND compared to EMP-LON (7.61 m). Compared to EMP-LON, both $\frac{H}{W}$ and $\frac{W}{R}$ are smaller using EMP-IND, indicating that EMP-IND generates wide spread relatively smaller size buildings (Figure A.2). For wide canyons ($\frac{H}{W} <= \frac{1}{3}$), the buildings are well spaced and they act as isolated roughness elements.

MORUSES-IND and MORUSES-LON differ only in terms of empirical fit used for the derivation of urban morphology data and Figure A.3 clearly describes the difference between the derivation of urban morphology data between the two experiments. MORUSES scheme needs three input parameters, namely, λ_f, λ_p and H. These parameters are retrieved from Very High Resolution (VHR) optical satellite stereo data of Pleiades 1A/1B (0.5 m resolution stereo) over the urban areas of Delhi where the data is present. Since these variables are not available over the entire urban area within the study domain of Delhi, empirical relationships are derived using these retrieved parameters and the urban fraction by employing the method described

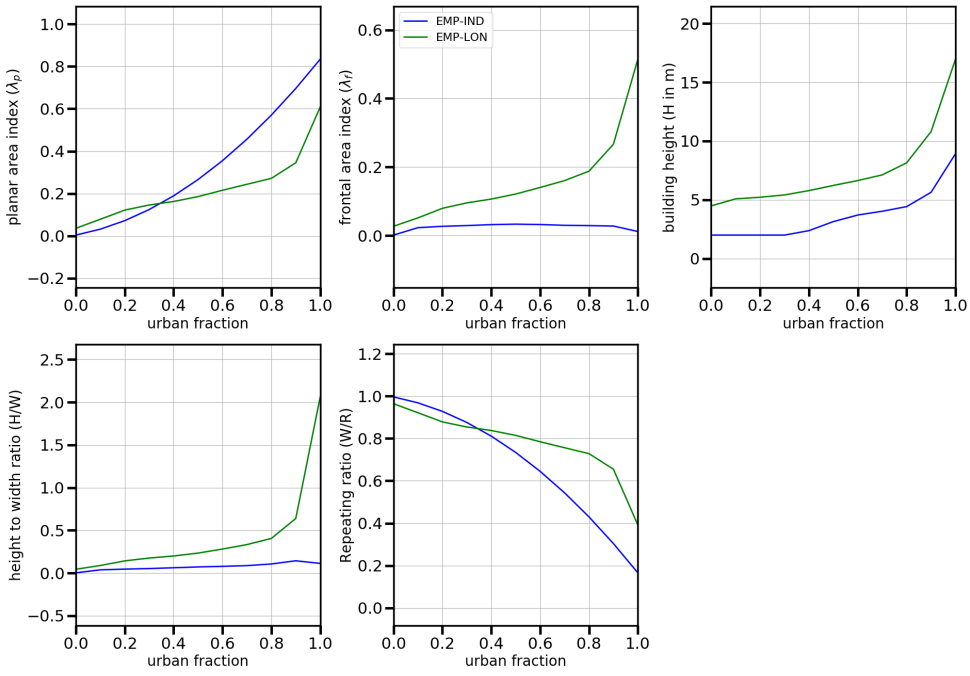

FIGURE 3 Urban morphology parameters (a) planar area index (b). frontal area index (c) building height (d) height to width ratio and (e) repeating with a ratio based on EMP-IND and EMP-LON as a function of the urban fraction. Urban fraction varies between 0 and 1. EMP-IND and EMP-LON correspond to the empirical relationship based on Indian and London data respectively

by Bohnenstengel et al. (2011). As described in equations 5, 6 and 7 , these newly derived empirical relationships are function of urban fraction only and hence can be easily derived in a NWP model where urban fraction is an input parameter as part of its surface definition. In MORUSES-IND experiment, λ_f, λ_p and H are determined from the urban fraction based on CCI LULC over the Delhi domain using these newly derived empirical fits (Equation 5,6 and 7 in section 2.2.2). In the case of MORUSES-LON experiment, these urban parameters are determined with another empirical fit (See equations 12, 13 and 14), which is also a function of urban fraction (Bohnenstengel et al., 2011). These empirical fits are used here because these are the default empirical relationships in the MORUSES scheme and the only available empirical fit for the urban morphology data using the similar approach. Though these empirical fits are derived based on London urban data, they provide an opportunity to understand the difference in the urban morphology between different cities and their impact in the numerical simulations.

$$\lambda_p = 22.88fu^6 - 59.47fu^5 + 57.75fu^4 - 25.11fu^3 + 4.33fu^2 + 0.19fu + 0.036 \quad (12)$$

The λ_f is defined as

$$\lambda_f = 16.41fu^6 - 41.86fu^5 + 40.39fu^4 - 17.76fu^3 + 3.24fu^2 + 0.06fu + 0.0271 \quad (13)$$

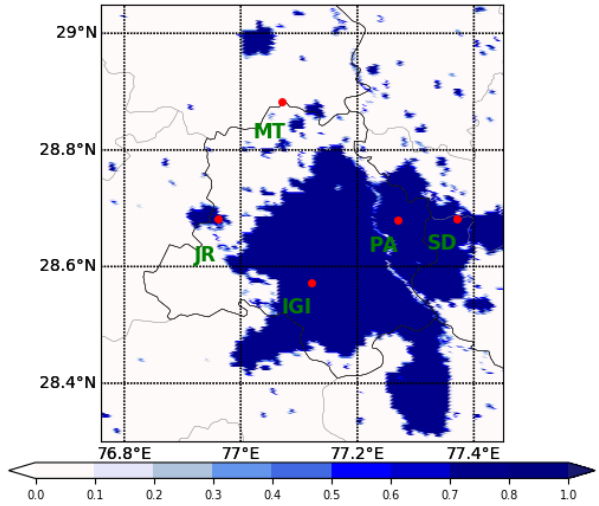

FIGURE 4 Urban fraction derived based on CCI for the model domain. Here JR, IGI, PA and SD represent the urban observations sites, while MT corresponds to a rural observation location used in the present study for verification.

and the H is derived as

$$H = 167.409fu^5 - 337.853fu^4 + 247.813fu^3 - 76.3678fu^2 + 11.4832fu + 4.48226 \quad (14)$$

.2 | Appendix B

In order to understand the spatial impact of MORUSES-IND, the difference between MORUSES-IND and BEST-1t at 14 UTC are examined on a typical clear day, 25/11/2016 (Figure A.4) and a typical fog day, 22/01/2016 (Figure A.5) respectively. An extremely dense fog event occurred on 22nd to 23rd January 2016 which is characterized by very low visibility, less than 50 m, for almost 3-4 hours and very low wind speeds. An overview of the fog day is presented in Ghude et al. (2017). It should be noted that the magnitudes of Q_H are negative at 14 UTC. Hence in comparison with BEST-1t, MORUSES-IND yield more/less downward Q_H depending upon whether δQ_H is negative/positive. Spatial difference plot on the clear day shows that MORUSES-IND reduces the magnitudes of all the variables over the urban area except wind speed and Q_H (Figure A.4). The positive magnitudes of δws show the large magnitudes of wind speed using MORUSES-IND while the values of δQ_H demonstrate more downward sensible heat flux. $\delta L \uparrow$ shows that MORUSES-IND has feedback on the rural area around the city with increasing $L \uparrow$ over the non urban area. T_{screen} simulation is up to $\sim 2\,^{\circ}C$ cooler in MORUSES-IND (Figure A.4). δT_{skin} also exhibits a cooling tendency however the magnitudes are very small. This mainly results from the balance between more outgoing net long wave radiation Q_L and more incoming Q_H in MORUSES-IND. As we have seen in clear day, surface and atmosphere coupling via skin and T_{screen} is similar on the fog day where both δT_{screen} and δT_{skin} are lower indicating the MORUSES-IND simulations are colder at 14 UTC. However, on the fog day the difference between these variables is up to $\sim 4\,^{\circ}C$. Similarly, $\delta L \uparrow$ is up to 20 $W m^{-2}$ smaller in MORUSES-IND. MORUSES-IND produces relatively less outgoing net Q_L at 14 UTC due to the reduction in both Q_L components (Figure A.5). Depending upon the time chosen, the sign and the magnitudes of the variables can vary, however the plots display the impact of MORUSES spatially over the urban area and the surroundings.

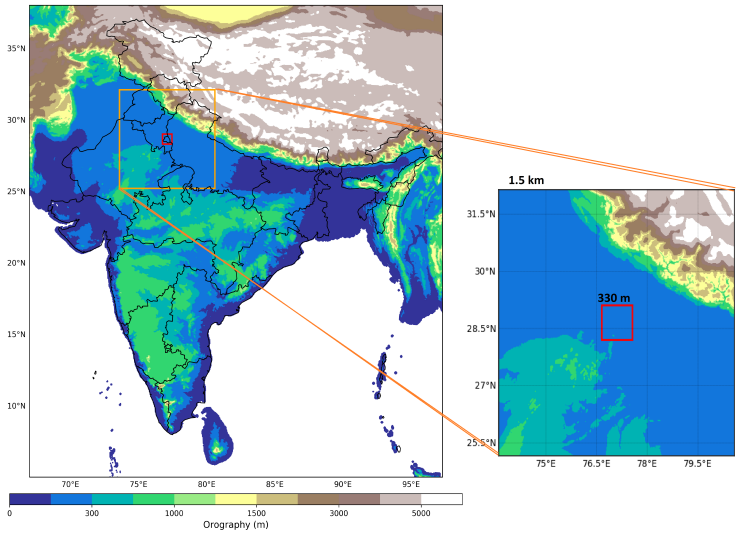

FIGURE 5 Topography and the schematic of the DM nested configurations used in the numerical experiment. The zoomed image shows the nested 1.5 km and 330 m model domains.

It is not possible to state definitive conclusions after the analysis of a single time/case. Nevertheless, it can be pointed out that the impact of MORUSES-IND is more or less uniform over the urban area as a result of the rather homogenous land surface data and the effect is more pronounced on the fog day. The increased wind speed and the cooling of screen as well as skin temperatures over the urban area again indicate that MORUSES-IND more accurately represents the impact of urbanization which appears exaggerated in the BEST-1t.

TABLE 1 Details of numerical experiments

Numerical experiments	Description
BEST-1t	1 tile default scheme using CCI LULC
MORUSES-IND	2 tile MORUSES scheme using CCI LULC & urban data based on EMP-IND
MORUSES-LON	2 tile MORUSES scheme using CCI LULC & urban data based on EMP-LON

TABLE 2 Summary of clear and fog events used in the current analysis with dates. Here minimum visibility and fog duration is estimated based on the IGI station. The duration of fog is determined for the period where visibility is less than 1 km

Clear sky days	Fog days	minimum visibility (m)	fog Duration (hrs)
2016-11-25	2016-01-21	<= 100	9
2016-11-26	2016-01-22	<= 100	16
2016-11-27	2016-02-08	<=100	13
2016-11-28	2016-02-09	<= 100	9
2017-11-22	2016-12-04	800	4
2017-11-23	2016-12-05	800	4
2017-11-24	2016-12-06	<=100	15
2020-11-18	2016-12-14	<=100	10
2020-11-19	2016-12-15	300	6
	2018-01-28	<=100	9
	2018-01-29	<=100	8

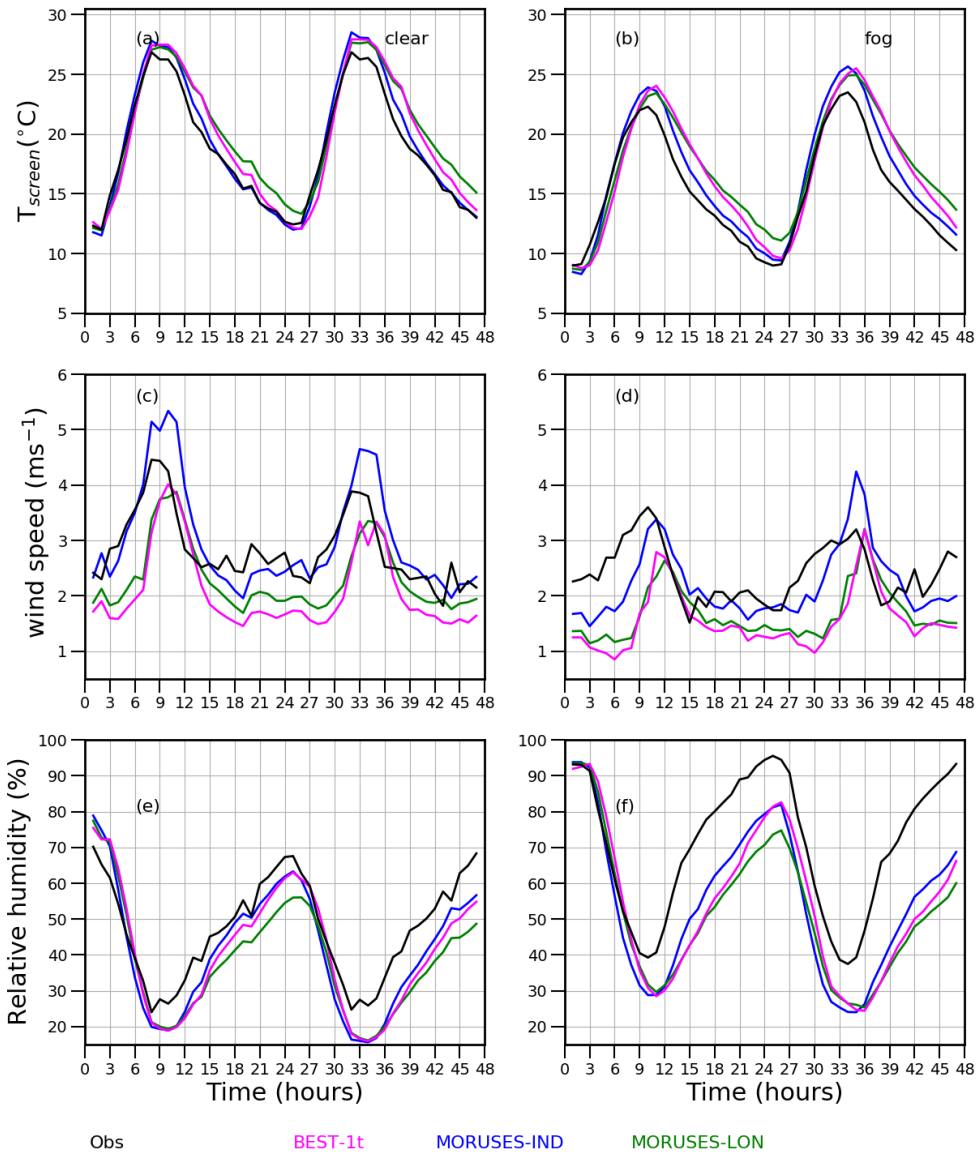

FIGURE 6 Ensemble mean diurnal cycle of observed (black) a-b screen temperature T_{screen} (^{o}C), c-d wind speed (ms^{-1}) and e-f relative humidity (%) are compared with the numerical simulations BEST-1t (magenta), MORUSES-IND (blue) and MORUSES-LON (green) at IGI, an urban site. Left and right columns show clear and fog cases respectively.

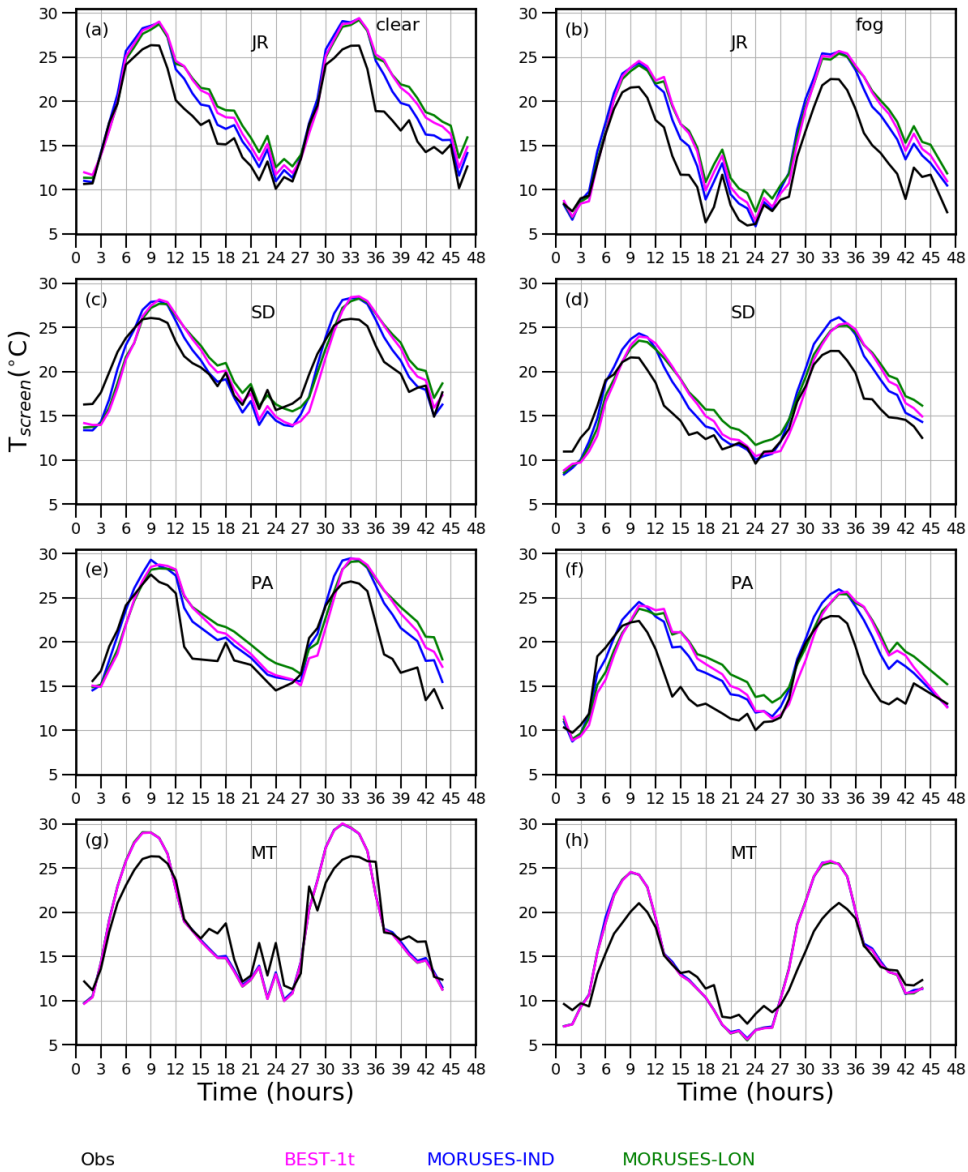

FIGURE 7 Ensemble mean diurnal cycle of observed screen temperature $T_{screen}(^{o}C)$ at JR (a-b) , SD (c-d) PA (e-f) and MT (g-h) respectively are compared with the numerical simulations BEST-1t (magenta), MORUSES-IND (blue) and MORUSES-LON (green). Left and right columns show clear and fog cases respectively. Here JR, SD and PA are urban locations while MT is a rural site.

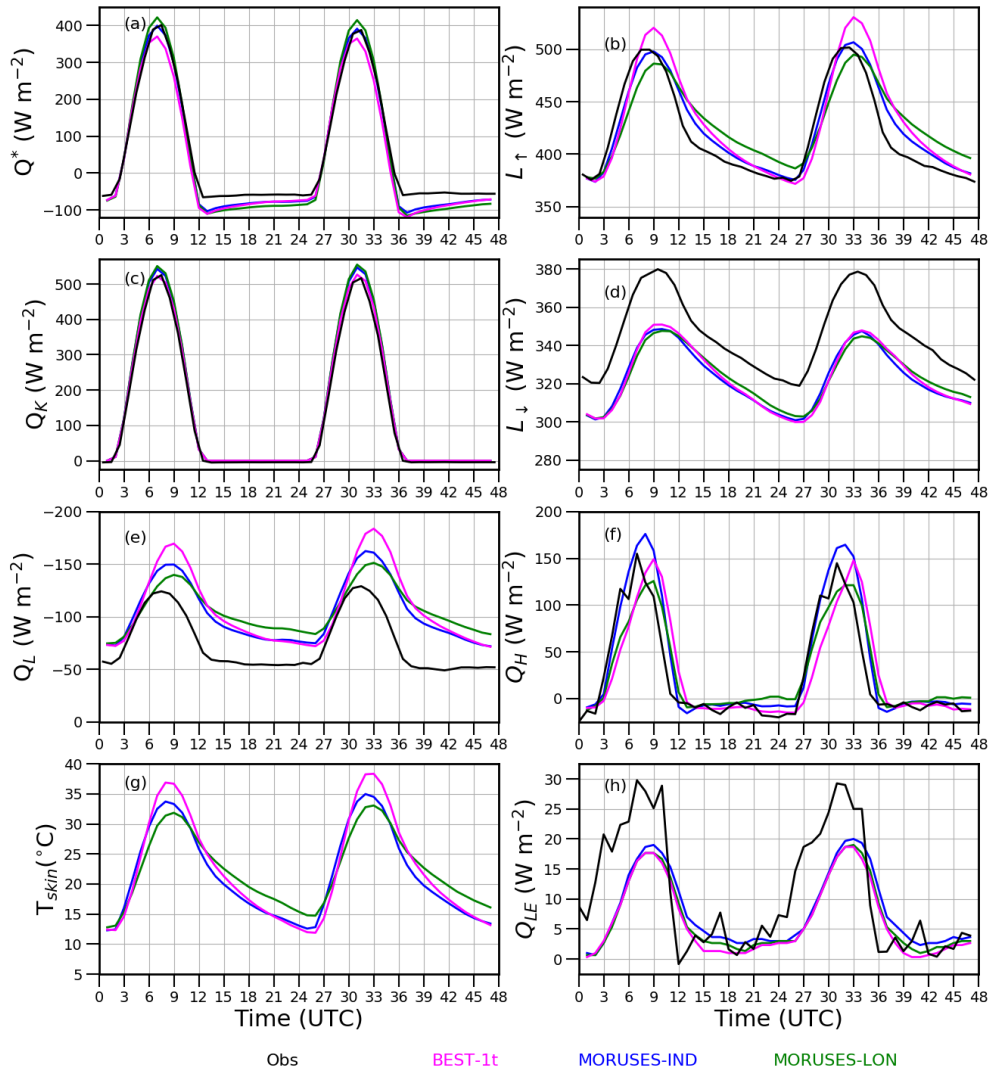

FIGURE 8 Ensemble mean diurnal cycle of simulated (a) net radiation Q^* (Wm^{-2}) (b) up welling long wave $L_{\uparrow}$ (Wm^{-2}) (c) net shortwave radiation Q_K (Wm^{-2}) (d) down welling long wave $L_{\downarrow}$ (Wm^{-2}) (e) net long wave radiationQ_L (Wm^{-2}) (f) sensible heat flux Q_H (Wm^{-2}) (g) skin temperature T_{skin} (^{o}C) and (h) latent heat flux Q_{LE} (Wm^{-2}) using BEST-1t (magenta), MORUSES-IND (blue) and MORUSES-LON (green) are compared with the observations at IGI, an urban site for clear sky conditions

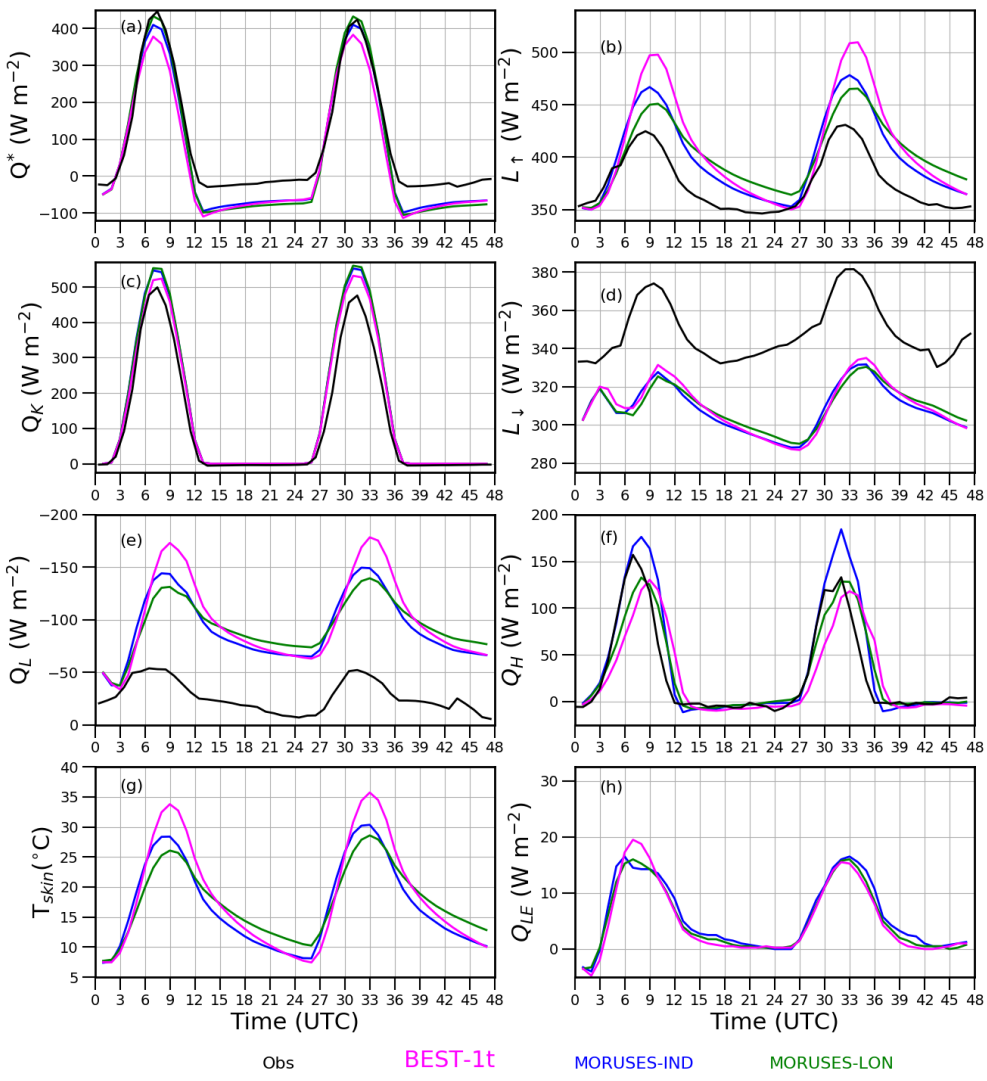

FIGURE 9 Same as Figure 8 but for foggy conditions at IGI, an urban site

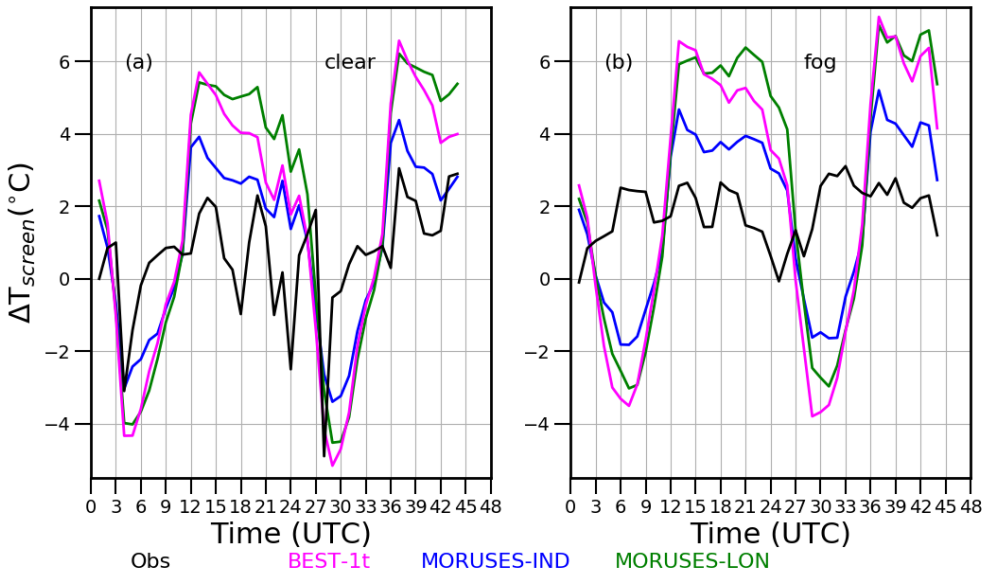

FIGURE 10 Ensemble mean diurnal cycle of observed (black) ΔT_{screen} (^{o}C) are compared with the three numerical simulations. Here Δ represents the difference between IGI, an urban site and MT a rural site. Left and right columns show clear and fog cases respectively.

TABLE 3 RMSE and mean bias of T_{screen} (^{o}C), wind speed ws (ms^{-1}) and relative humidity (%) for clear and foggy days at IGI.

Variable	Numerical experiments	RMSE		Mean bias	
		Clear	Fog	Clear	Fog
T_{screen} (°C)	BEST-1t	1.92	2.75	0.84	1.5
	MORUSES-IND	1.36	1.95	0.46	1.17
	MORUSES-LON	2.11	2.93	1.35	1.98
ws (m s^{-1})	BEST-1t	1.14	1.36	-0.65	-0.89
	MORUSES-IND	0.97	1.12	0.41	-0.09
	MORUSES-LON	1.0	1.3	-0.41	-0.74
relative humidity	BEST-1t	11.8	23.25	-6.2	-16.6
(%)	MORUSES-IND	11.1	21.3	-6.0	-16.2
	MORUSES-LON	13.7	25.1	-8.7	-18.94

TABLE 4 RMSE and mean bias of T_{screen} for clear and foggy days over urban loactions JR, SD and PA respectively.

Variable	Numerical experiments	RMSE		Mean bias	
		Clear	Fog	Clear	Fog
JR	BEST-1t	3.19	4.69	2.57	2.4
	MORUSES-IND	2.47	4.7	2.0	2.4
	MORUSES-LON	3.3	4.68	2.75	2.6
SD	BEST-1t	2.9	3.3	-0.13	1.25
	MORUSES-IND	2.3	2.9	0.02	1.5
	MORUSES-LON	2.7	3.3	0.35	1.75
PA	BEST-1t	3.6	3.6	1.3	1.2
	MORUSES-IND	2.9	3.1	1.6	1.9
	MORUSES-LON	3.6	3.5	1.6	1.9

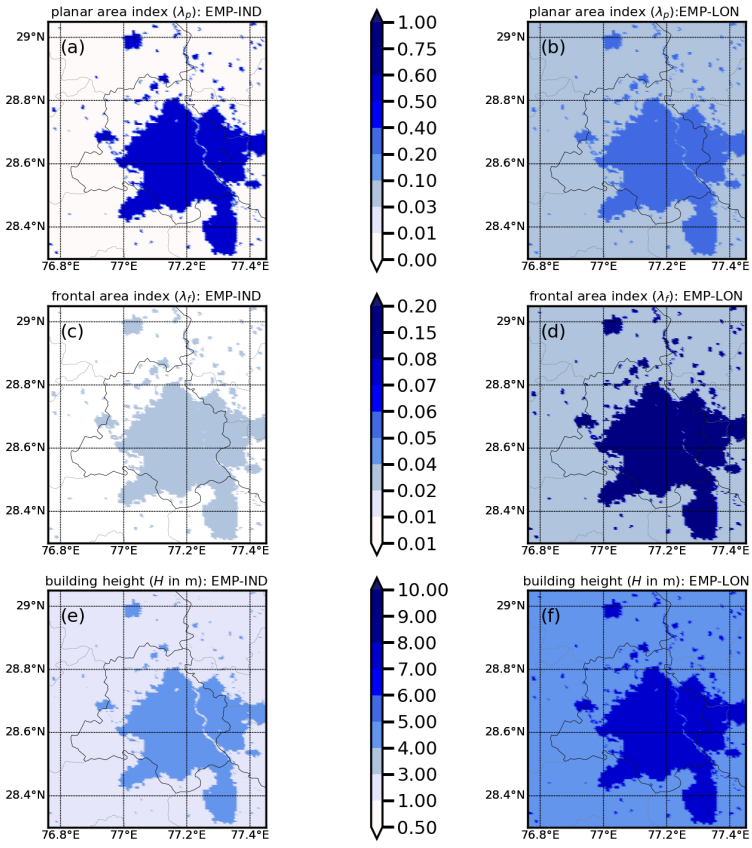

FIGURE A.1 Planar area index (a-b), frontal area index (c-d) and building height (e-f) based on EMP-IND and EMP-LON using CCI land cover data.

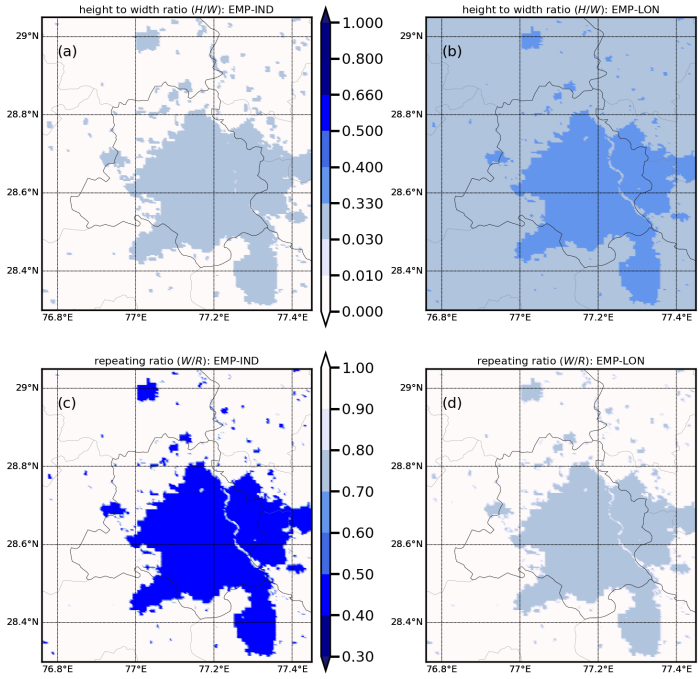

FIGURE A.2 Height to width ratio (a-b) and repeating width ratio (c-d) based on EMP-IND and EMP-LON using CCI land cover data.

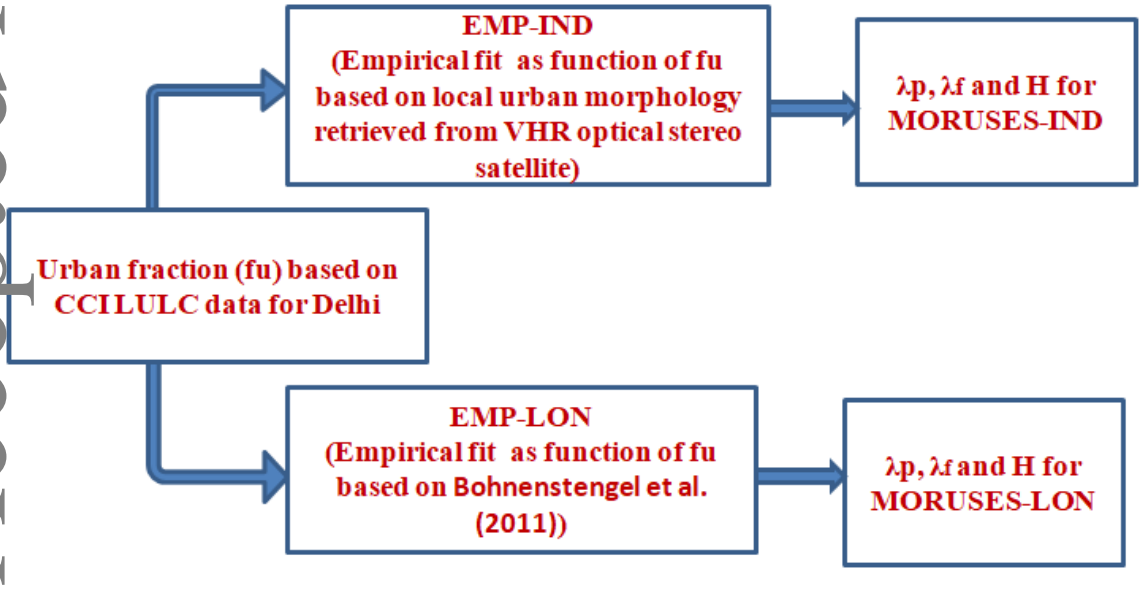

FIGURE A.3 A schematic representing the difference in the derivation of urban morphology data in MORUSES-IND and MORUSES-LON experiments

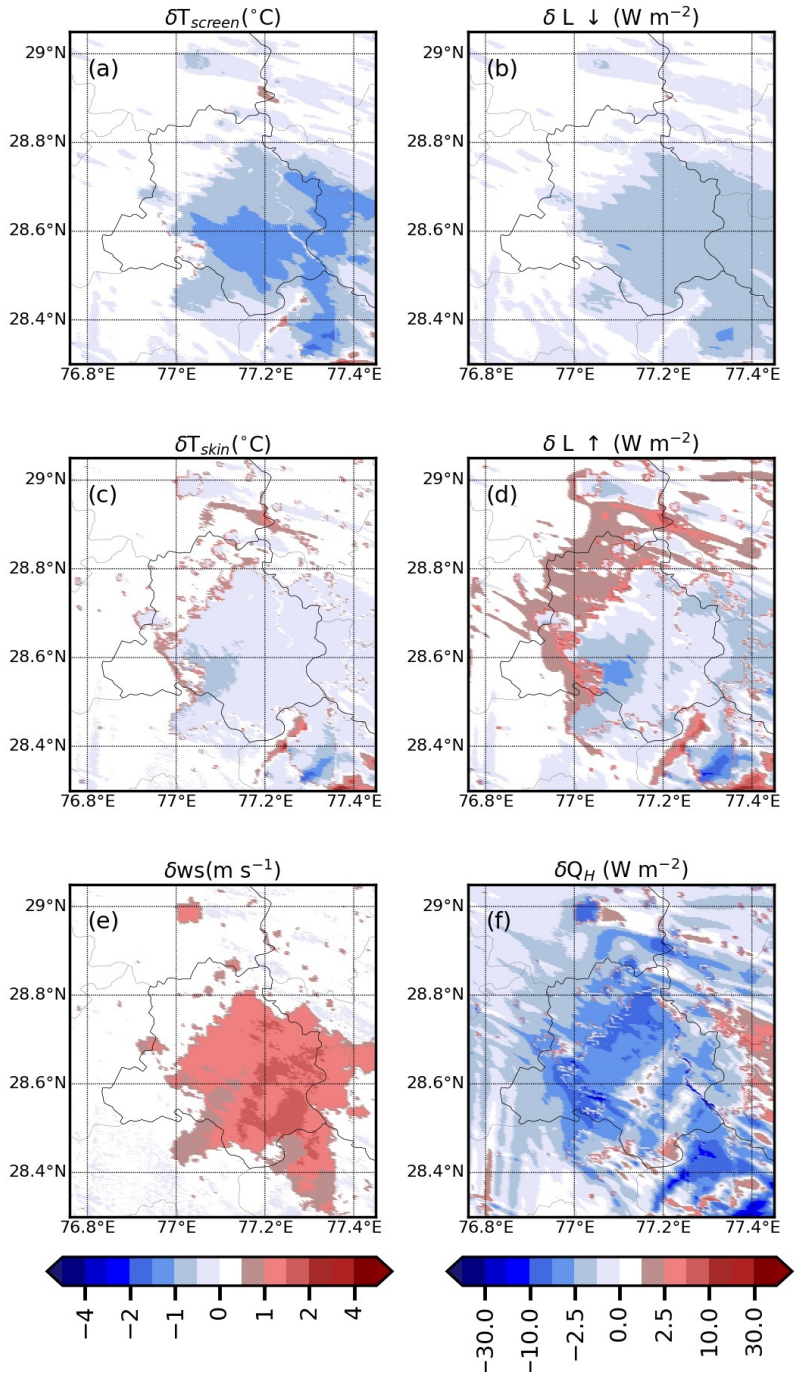

FIGURE A.4 Spatial plot of (a) δ T$_{screen}$ (^oC)(b) δ L$_{\downarrow}$ (Wm^{-2}) (c) δ T$_{skin}$ (^oC) (d) δ L$_{\uparrow}$ (Wm^{-2}) (e) δ ws (ms^{-1}) and (f) δ Q$_H$ (Wm^{-2}) at 14 UTC. Here δ represents the difference between MORUSES-IND and BEST-1t for different parameters on a clear day (25/11/2016).

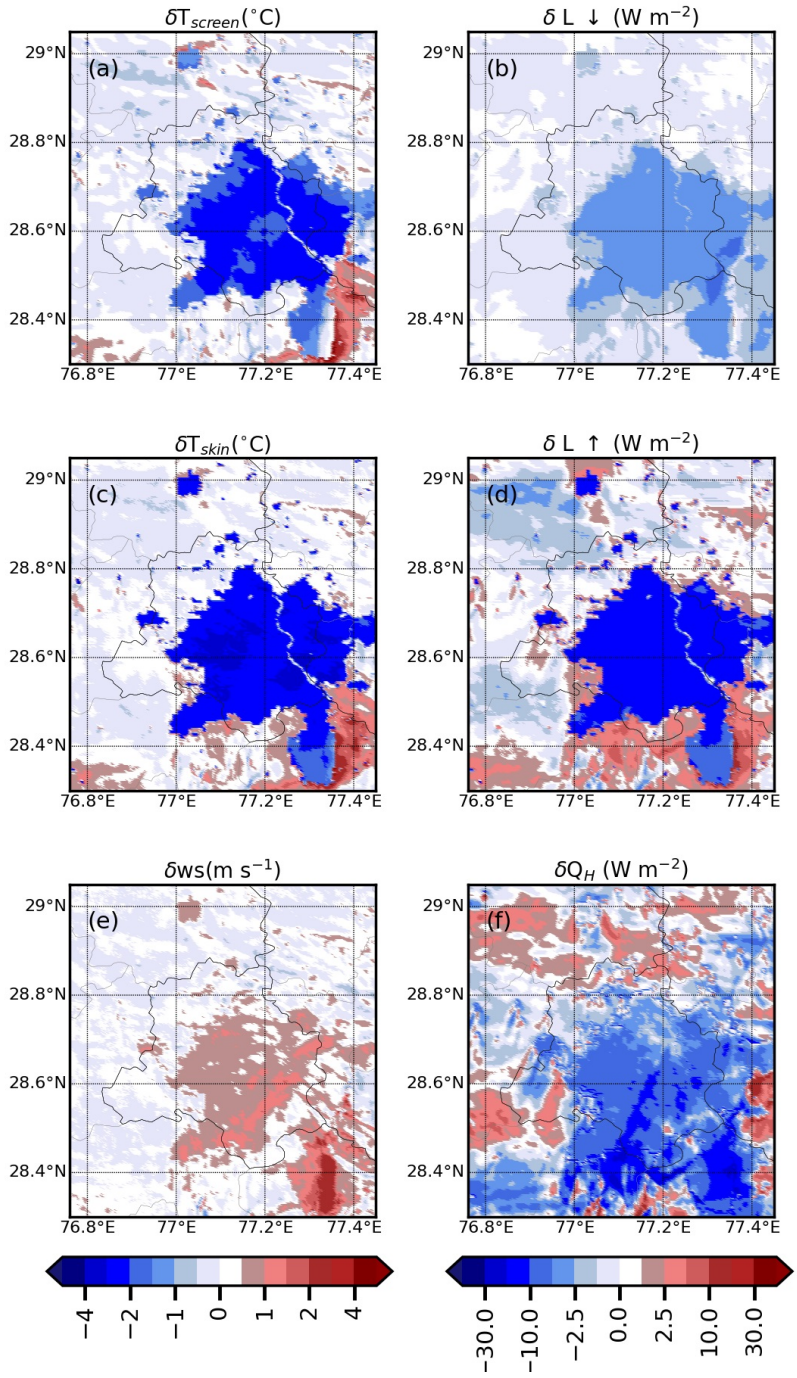

FIGURE A.5 Same as figure A.4 but on a typical fog day (22/01/2016) at 14 UTC. Here δ represents the difference between MORUSES-IND and BEST-1t for different variables.